Revision 1

CO_2 quantification in silicate glasses using µ-ATR FTIR spectroscopy

Word Count: 7008

Maximilian Schanofski[*1], Lennart Koch[1], Burkhard C. Schmidt[1]

[1]Abteilung Experimentelle und Angewandte Mineralogie, Georg August Universität Göttingen, Goldschmidtstraße 1, 37077 Göttingen

[*] Corresponding author.

E-mail: m.schanofski@gmx.de

Phone: 0049-551/39 33871

Fax: 0049-551/39 3863

Key words: ATR-micro spectroscopy, ATR FTIR, silicate glasses, carbon dioxide, CO_3^{2-} quantification, CO_2

Abstract

A new method for measurements of high CO_2 concentrations in silicate glasses was established using micro–Attenuated Total Reflectance (µ-ATR) Fourier transform Infrared (FTIR) spectroscopy in the mid-IR (MIR) region. We studied two glass/melt compositions, namely leucitite and granite, to cover samples in which CO_2 is dissolved as carbonate ions (CO_3^{2-}) or as CO_2 molecules (CO_2^{mol}). In the leucitite glasses a carbonate absorption doublet with maxima at 1510 and 1430 cm^{-1} has shown to clearly separate from aluminosilicate lattice vibrations at lower wavenumbers. Due to the lower

This is the peer-reviewed, final accepted version for American Mineralogist, published by the Mineralogical Society of America.
The published version is subject to change. Cite as Authors (Year) Title. American Mineralogist, in press.
DOI: https://doi.org/10.2138/am-2022-8477. http://www.minsocam.org/

sensitivity of the μ-ATR method, we were able to measure high CO_2 contents (c_{CO2} > 0.5 wt%) in experimental silicate glasses that would only be measurable with great difficulties using established transmission MIR measurements due to detector linearity limit effects even with very thin sample wafers. The peak heights of the 1430 cm^{-1} ATR band (A_{1430}), normalized to the integral of the T-O lattice vibrations (T = Si, Al, Fe) at about 930 cm^{-1} (Int_{930}) show a linear trend with CO_2 contents in the range 0.2 - 4.3 wt%, yielding a linear correlation with c_{CO2} [wt%] = 0.4394±0.006 * A_{1430} * 10000 / Int_{930}. The normalization of the CO_2 related band to a lattice vibration accounts for variations in the quality of contact between ATR crystal and sample, which has a direct effect on signal intensity. In granitic glasses, where CO_2 is dissolved as CO_2^{mol} only, the asymmetric stretching vibration at 2350 cm^{-1} overlaps with the signal of atmospheric, gaseous CO_2. As the ATR signal of dissolved CO_2 is very weak, the atmospheric signal may dominate the spectrum. Since the absorbance spectrum is calculated by division of the single channel sample spectrum by a single channel reference spectrum measured in air, keeping the laboratory and spectrometer atmosphere as constant as possible during spectral acquisition can resolve the problem. Nonetheless, a procedure to subtract the signal of remaining atmospheric CO_2 may still be required for the spectral evaluation. We studied a series of 5 granitic glasses with CO_2^{mol} contents of 0.08 to 0.27 wt% and found an excellent linear relation between CO_2 concentration and lattice vibration normalized ATR intensity of the 2350 cm^{-1} band: c_{CO2} [wt%] = 0.2632±0.0016 * A_{2350} * 10000 / Int_{990}. Although the CO_2^{mol} concentrations in our granitic glass series can still be analyzed without major difficulties by conventional transmission IR spectroscopy, our data demonstrate the potential of the ATR method for samples with higher CO_2 contents or for samples where a high spatial resolution is required (melt inclusions, vesicular or partially crystallized glasses). The lower limits of the ATR method are approximately 0.2 wt% CO_2 dissolved as carbonate groups or 0.1 wt% CO_2 (or slightly less) dissolved in molecular form.

This is the peer-reviewed, final accepted version for American Mineralogist, published by the Mineralogical Society of America.
The published version is subject to change. Cite as Authors (Year) Title. American Mineralogist, in press.
DOI: https://doi.org/10.2138/am-2022-8477. http://www.minsocam.org/

Introduction

Besides water, carbon dioxide is the second most abundant volatile in magmatic systems (e.g. Anderson 1975; Symonds et al. 1994; Johnson et al. 1994). Silicate melts play a fundamental role in transporting carbon from the Earth's interior to its surface. However, in most silicate melts CO_2 solubility is one to two orders of magnitude lower than the solubility of water under equivalent conditions (e.g. Mysen et al. 1976; Blank et al. 1993; Holloway and Blank, 1994; King and Holloway 2002; Lesne et al. 2011a, b; Iacono-Marziano et al. 2012; Shishkina et al. 2014; Fanara et al. 2015; Schanofski et al. 2019). Several analytical methods exist to quantify CO_2 concentration in silicate glasses: Infrared and Raman spectroscopy, elemental carbon analysis and secondary ion mass spectrometry.

The most frequently used spectroscopic method to analyze CO_2 concentration in silicate glasses is Fourier-transform infrared (FTIR) spectroscopy (see Ni and Keppler 2013, for review and references). It is a vibrational spectroscopic technique recording the interaction of electromagnetic radiation with structural units at the molecular level, more specifically, the absorption of the infrared radiation. In the case of silicate glasses, the asymmetric stretching vibrations of CO_2 dissolved in the molecular form (CO_2^{mol}) and as carbonate groups (CO_3^{2-}) are well separated from the absorbance bands of the glass matrix (e.g. Mysen et al. 1976; Fine and Stolper, 1985; Blank and Brooker, 1994). The quantification of CO_2^{mol} and CO_3^{2-} is done by correlating the baseline subtracted absorbance (measured in transmission on doubly polished sections with known thickness) to the concentration using the Lambert-Beer law. This method however requires a calibration by an independent absolute method such as elemental carbon analysis for each melt composition. Moreover, it is limited to low CO_2 concentrations due to strong absorbance and the related detector saturation or non-linearity, even when using very thin sample wafers (Fig. 1). Altogether, this technique has many advantages: it is non-destructive, measures concentrations down to ppm level

and delivers information on molecular CO_2 and CO_3^{2-} groups in the analyzed glass. In addition, FTIR spectroscopy can also measure the H_2O content and speciation in silicate glasses simultaneously.

A few studies applied reflectance FTIR spectroscopy to measure CO_2 contents (dissolved as CO_2^{mol} and CO_3^{2-}) in silicate glasses (Grzechnik et al. 1996; Moore et al. 2000; King and Larsen 2013). This technique requires only a single sample surface to be polished, and no thickness measurement is required. Spectral parameters from the reflection spectra and from Kramers-Kronig transformed spectra were used for empirical quantification. The method is intended for samples that are difficult or impossible to be prepared for transmission measurements (e.g. small melt inclusions, cracked, vesicular or crystal bearing glasses), and is not restricted to lower CO_2 concentrations due to smaller intensities of reflectance spectra compared to transmission data.

Morizet et al. (2013) established an empirical calibration for the quantification of CO_2 in geologically relevant glasses (in which CO_2 dissolved as carbonate groups) using confocal micro-Raman spectroscopy. They reported a linear dependence between the normalized peak areas of the carbonate vibrations at 1062 - 1092 cm^{-1} and the CO_2 concentration determined by elemental carbon analysis or FTIR spectroscopy. The spectral evaluation is complex, as T-O stretching vibrations (T = Si, Al, Fe^{3+} in tetrahedral coordination) of the aluminosilicate network superimpose the carbonate signal. Therefore, multiple Gaussian peaks are fitted to this high-frequency region in an iterative process after applying a third order polynomial baseline to separate the carbonate signal from that of the aluminosilicate network. However, there is no calibration available for CO_2 dissolved as CO_2 molecules, as in silicic melts. Raman spectroscopy has a high spatial resolution and requires only single polished samples. The calibration of Morizet et al. (2013) was established for CO_2 concentrations between 0.2 and 16 wt% with a reported accuracy of better than 0.4 wt% CO_2.

Secondary ion mass spectrometry (SIMS) was used in several studies as analytical method for CO_2 in various silicate glasses (e.g. Pan et al. 1991; Thibault and Holloway 1994; Hauri et al. 2002;

This is the peer-reviewed, final accepted version for American Mineralogist, published by the Mineralogical Society of America.
The published version is subject to change. Cite as Authors (Year) Title. American Mineralogist, in press.
DOI: https://doi.org/10.2138/am-2022-8477. http://www.minsocam.org/

Behrens et al. 2004a). SIMS uses an ion beam focused on the surface of the sample. The incoming ions spatter ionized atoms from the surface of the sample, which are collected and analyzed by a mass spectrometer. The abundance of carbon is calculated from the empirical linear correlation between the count rates of ^{12}C normalized to those of ^{28}Si-, and the concentration of CO_2 in standards. This technique is also dependent on an initial standardization using another technique.

One of the most frequently used independent methods to measure bulk CO_2 concentration is elemental carbon analysis with a combustion analyzer (e.g. Thibault and Holloway 1994; Brooker et al., 1999, 2001a; Morizet et al., 2002; Behrens et al 2009; Fanara et al. 2015; Moussallam et al., 2015). It is often combined with sulfur analysis to a so-called "carbon-sulfur analyzer" (CSA). The sample is combusted at high temperatures in a stream of oxygen gas to release all carbon in the form of molecular CO_2. Its abundance is then determined by an infrared cell. CS-analysis is a widely used technique in experimental petrology for characterization of standards for other methods or for bulk rocks. The measurement is a destructive but sensitive technique that requires a relatively high amount of material (approx. 5 - 50 mg depending on CO_2 concentration in the sample).

In this study, we applied micro-Attenuated Total Reflectance (µ-ATR) FTIR spectroscopy to quantify CO_3^{2-} and CO_2^{mol} contents in CO_2-bearing glasses on the example of leucititic and granitic melts. This method was previously applied to the quantitative analysis of water in silicate glasses (Lowenstern and Pitcher 2013; Amma et al. 2016; Allabar and Nowak 2020), but nor for CO_2. Although the µ-ATR-FTIR technique is less sensitive than normal transmission FTIR spectroscopy, it can be very useful in the case of high CO_2 contents. It can also be valuable to quantify CO_2 contents in vesiculated samples or glass inclusions within crystals, since its penetration depth is only few µm and is capable of measuring spots of diameters down to approx. 5 µm. In addition, it simplifies the sample preparation, since only one side of the glass sample needs to be polished. This method can be

This is the peer-reviewed, final accepted version for American Mineralogist, published by the Mineralogical Society of America.
The published version is subject to change. Cite as Authors (Year) Title. American Mineralogist, in press.
DOI: https://doi.org/10.2138/am-2022-8477. http://www.minsocam.org/

120 applied to glasses with CO_3^{2-} concentration down to about 0.2 wt% CO_2 and for CO_2^{mol} contents
121 down to about 0.1 wt% CO_2.
122
123 **Methods**
124 **Sample preparation**
125 For our study, we synthesized a crystal and bubble free leucitite glass of the "SULm" composition
126 from Freda et al. (2011). Synthesis conditions and procedures of this glass are given in detail in
127 Schanofski et al. (2019). The composition and homogeneity of the glass were checked using a
128 Bruker™ M4 Tornado micro-X-ray fluorescence (µ-XRF) spectrometer and are listed in Table 1. CO_2
129 bearing glasses were produced in high-pressure high-temperature experiments. For pressures
130 between 0.5 and 5 kbar the nominally dry starting glass powder was sealed together with $Ag_2C_2O_4$
131 as CO_2 source into $Au_{75}Pd_{25}$ capsules (4.0-3.6 mm diameter, 25 mm length) and was saturated with
132 CO_2 over 17-96 h in an internally heated pressure vessel (IHPV) at 1250 °C (Table 2). Hydrous glasses
133 containing 2.2 to 6.3 wt% water were synthesized in the same apparatus at 3 kbar by using a mixture
134 of $Ag_2C_2O_4$ and H_2O. IHPV experiments were terminated by drop quench, yielding quench rates of
135 about 150 °C/s. More details on these experiments can be found in Schanofski et al. (2019) and in
136 Table 2.
137 Experiments at higher pressures (9 – 18 kbar, 1375 °C, excess of $Ag_2C_2O_4$) were performed in Pt
138 capsules (4.0-3.6 mm diameter, 8 mm length) in an end-loaded piston cylinder (PC) apparatus using
139 talc-pyrex assemblies with crushable alumina plugs and sleeves and a graphite furnace. As we used
140 the same PC apparatus and assemblies as in Stalder (2004) we applied the same friction correction
141 of 10% to the nominal pressures to obtain the sample pressures. Further details on the experimental
142 setup of piston cylinder experiments and pressure calibration in our laboratory can be found in
143 Stalder (2004). Piston cylinder experiments ran for 0.5 to 22.5 hours and were terminated by

144 switching off the power of the furnace, yielding quench rates of about 120 °C/s as elaborated from
145 recordings of the temperature decrease of the thermocouple placed about 1 mm above the sample
146 capsule.
147 The sample capsules from piston cylinder experiments were cut parallel to the length axis using a
148 Well 3242 precision diamond wire saw with a 130 µm thick wire. The smaller part of the sample was
149 embedded in epoxy and polished on one side for µ-ATR FTIR measurements. The larger capsules
150 from IHPV experiments were unpacked with help of pliers and larger glass pieces were used to
151 prepare doubly polished glass sections. Final polishing for all our samples was done by 1 µm
152 diamond paste or corundum slurry.
153 A few CO_2 bearing granitic glasses were synthesized to test the applicability of the µ-ATR method to
154 quantitatively determine the CO_2 content of samples, where CO_2 dissolves in molecular form
155 (CO_2^{mol}). For these samples, anhydrous starting glasses, were prepared by melting natural granitic
156 rocks (Okertal granite (OTG) and Brocken granite from Knaupsholz quarry (GKH), both from Harz
157 Mountains, Germany) 3 times for 1-2 hours at 1 atm and 1600° C in a Pt crucible. These starting
158 glasses were sealed as powders and shards together with $Ag_2C_2O_4$ or $H_2C_2O_4*2H_2O$ into $Au_{75}Pd_{25}$
159 capsules (4.0-3.6 mm diameter, 20 mm length) by arc welding. In order to produce a bubble free
160 portion in these highly viscous melts, which is suitable for FTIR transmission analysis, a small bubble
161 free starting glass block of about 2-3 mm diameter was placed in the lower part of the capsule and
162 was surrounded by glass powder. The samples were saturated with CO_2 or mixed CO_2-H_2O fluids at
163 2 to 5 kbar in an IHPV using the same procedures as for the leucitite glasses. Melts quenched to
164 crystal free, but bubble containing glasses. Glass compositions and experimental details are given
165 in Tables 1 and 3.
166

167 **CSA Measurements**

The determination of infrared absorption coefficients or correlation factors for quantitative infrared analysis requires samples with known concentrations of the species in question. For CO_2 in the leucitite glasses we used an Elementar™ Inductar CS cube carbon sulfur analyzer (CSA). Details of the analytical procedure are given in Schanofski et al. (2019). Since bubbles trapped in the CO_2 saturated glass would dramatically increase the measured CO_2 content, the glassy samples were ground to a coarse powder to crack open existing CO_2 bubbles. The powder was checked for remaining closed bubbles in transmitted light using a stereo microscope with 40x magnification. The powder was stored in a drying furnace over night to crack open any residual bubbles by overpressure of the trapped volatile phase at 130 °C. The analyzed sample masses ranged between 7 and 50 mg per measurement, depending on the amount of available material and estimated CO_2 content in comparison to the detection limit of the CSA. Two to eight repeated measurements were performed for each sample to obtain mean CO_2 concentrations and a corresponding 2σ error (see Table 2). Independent CO_2 measurements with the carbon sulfur analyzer were not performed on granitic glasses due to numerous small bubbles in major parts of the glass bodies.

Infrared spectroscopy

All Fourier Transform Infrared (FTIR) measurements were performed with a Bruker™ Vertex 70 FTIR spectrometer coupled with a Bruker™ Hyperion 3000 IR microscope. For the mid-infrared (MIR) region, the spectrometer is equipped with a Globar light source, a KBr beam splitter and a liquid N_2 cooled MCT detector at the microscope. The spectrometer and the closed parts of the microscope were purged with dried and CO_2-reduced air generated by an Ekom™ DK50 Plus adsorption air drier, but the open parts of the microscope (sample stage, objectives, condenser lens) were still subject to the laboratory atmosphere. Microscope MIR FTIR measurements were performed in 32 scans in the range 4000 to 600 cm^{-1} with a spectral resolution of 4 cm^{-1}. Measurements are performed in

two steps. First a reference spectrum is measured in air (single channel reference, I_0) and subsequently the sample spectrum (single channel sample, I) is acquired with identical acquisition parameters. The absorption spectrum (A) is then calculated as $A = -\log(I/I_0)$. The MCT detector has a linear response between 0 and at least 2 absorbance units (AU) and was determined by measuring various layers of 1.5 µm thin Mylar foils (Fluxana Mylar X-ray film sheets TF-115-345) with increasing cumulative thicknesses. For this test we started measuring a single layer of Mylar film in transmission, successively increasing the number of layers to 8. The evaluation of the peak height of the 1342 cm^{-1} band as function of the cumulative layers yields a linear trend up to 2 absorbance units. This linearity trend was confirmed by measuring a series of doubly polished sections of polystyrene hard plastics. The evaluation of the intensities of several absorption bands (1747, 1872 and 1943 cm^{-1}) as function of sample thickness indicates a deviation from the linear trend above 2.2 absorbance units (see Fig. A1 in the electronic supplement).

For measurements in transmission, doubly polished glass sections were placed on a pinhole on the motorized xy-stage (Merzhäuser™ Scan 75x50) of the Hyperion microscope and were measured with help of a Cassegrainian 15x objective and a similar condenser lens below the sample. The beam size was adjusted by a knife-edge aperture to a rectangular area of about 100 x 100 µm. The thickness of doubly polished sections was determined by a Mitutoyo™ digital micrometer (3 µm accuracy). Details of thickness, density, intensity, water contents of transmission samples are provided in Tables 2 and 3. ATR FTIR measurements (Fahrenfort, 1961) were performed as micro-analytical technique using a Bruker™ single reflection 20x µ-ATR objective, which has a Germanium crystal with a truncated, circular tip (d= 100 µm). The Ge crystal has a refractive index of 4.01 and an average angle of incidence at about 28.5°. The IR beam is focused onto the tip of the Ge crystal and undergoes an attenuated total internal reflection on the contact surface with the sample. An evanescent field is generated that enters the sample (i.e. the medium with the lower refractive

index). This evanescent field has vector components in all spatial orientations and can therefore interact with dipoles in all orientations. Knowing the frequency dependent refractive indices of the ATR crystal (Ge) and the samples (basaltic and granitic glasses) in the relevant infrared range (Li 1993, Pollak et al. 1973) a penetration depth (d_p) of the beam can be calculated. As this penetration depth was defined as the depth at which the electric field is decreased to 1/e of its surface value, the actual sampling depth corresponds to about $3d_p$ (e.g. Mirabella Jr. 1985). Sampling depth values are calculated to be 2.4 µm at 1430 cm^{-1} for the leucititic and 1.5 µm at 2350 cm^{-1} in the granitic glass. The beam diameter in the ATR crystal is about 32 µm but can be further reduced by the knife-edge aperture.

Carbon adhesive tape pads, typically used for SEM applications were used to fix the epoxy embedded samples on the microscope stage to prevent the sample from shifting during movement of the sample stage. Doubly polished glass sections (leucitite glasses synthesized at pressures up to 5 kbar and granite glasses) were placed on a glass slide that was stuck to the carbon adhesive tape pads. The beam size was set to 30 x 30 µm. At the ATR objective, force levels from 1 - 5 can be chosen for the contact pressure of the Germanium crystal with the sample, reflecting a contact force of 0.5 - 8 N. We found a level of 3 to be sufficient for a reliable contact and reproducible peak heights in our epoxy embedded silicate glasses as well as for doubly polished sections placed on glass slides. This force level was determined by collecting spectra of a sample (at identical sample spot) with all levels and measuring the peak heights and integral intensities of the 1430 cm^{-1} carbonate band and the 930 cm^{-1} T-O (T = Si, Al, Fe) stretching vibration, respectively (Fig. 2). These measurements reveal, that up to force level 3 the intensities increase and then level off (Fig. A2, electronic supplement), indicating that optimum contact is reached. The data also demonstrate, that our normalization procedure (see below) is capable to compensate small variations in contact quality.

This is the peer-reviewed, final accepted version for American Mineralogist, published by the Mineralogical Society of America.
The published version is subject to change. Cite as Authors (Year) Title. American Mineralogist, in press.
DOI: https://doi.org/10.2138/am-2022-8477. http://www.minsocam.org/

It should be noted here, that at higher force levels than 3, thin, free standing glass sections may break due to the force applied onto the sample.

Spectra were evaluated using the Bruker™ OPUS 7.5 software for baseline correction and intensity determinations (peak heights or integral intensities). Spectral scaling and subtraction procedures for the granitic glasses were performed with the Horiba™ Labspec 5 software due to more comfortable spectra manipulation features of this software. A detailed explanation of the baseline subtraction techniques can be found in the results section.

Results and discussion

Experimental Products

Leucititic samples synthesized in the IHPV were mostly bubble poor and crystal free. High pressure IHPV samples with a large amount of dissolved H_2O contained up to 10 vol% of micro quench crystals. Leucititic samples synthesized in PC experiments were bubble poor, contained a varying amount of nano-crystals, increasing with increasing pressure. Granitic glasses were crystal free and contained numerous bubbles in large parts of the glass body.

Carbonate groups in leucitite glasses

Transmission spectra of leucitite glasses showed no evidence for a peak at approx. 2350 cm^{-1} that would indicate the presence of molecular CO_2 (Fig. 1). A typical MIR ATR spectrum of a CO_2 rich leucitite glass is shown in Fig. 2. Carbonate groups dissolved in the silicate glass give rise to a doublet with maxima at 1510 and 1430 cm^{-1}, which results from v3 asymmetric stretching vibrations of distorted CO_3^{2-}groups (e.g. Blank and Brooker, 1994). It must be noted that the position of these maxima is shifting, depending on the composition of the glass (e.g. Blank and Brooker, 1994, Brooker

et al., 2001b). A linear baseline using two anchor points on both sides of the carbonate doublet (relative minima at 1260 to 1340 and about 1800 cm^{-1}) was applied to this doublet before measuring the peak height of the 1430 cm^{-1} vibration (A_{1430}) (Fig. 2). Lattice vibrations of the aluminosilicate network are situated below 1200 cm^{-1}. The peak with maximum at about 930 cm^{-1} results from T-O (T = Si, Al, Fe) stretching vibrations of network formers in tetrahedral coordination. The carbonate doublet is clearly separated from the lattice vibrations. Spectra showing the carbonate doublet for the entire series of anhydrous leucitite glasses covering 0.17 to 4.27 wt% CO_2 are given in Fig. 3. In particular for the samples with less than 1 wt% CO_2 (Fig. 3a) we frequently observe a distorted line shape of the high frequency band of the carbonate doublet, which often manifests in a sharp maximum at about 1510 cm^{-1}. The peak shape indicates a missing component just above 1510 cm^{-1} rather than an additional narrow component at 1510 cm^{-1} (e.g. due to presence of a crystalline phase). We think that this artefact is due to rotational vibrations of water molecules in the beam path that are not fully compensated by the division of the two single channel sample and reference spectra. In transmission spectra (Fig. A3, electronic supplement), in which the intensities of the carbonate doublet are at least one order of magnitude higher than in ATR spectra we rarely observe this effect (and if we do, it is much less pronounced). This perturbation of the high frequency band of the carbonate doublet leads us to the decision to only use the low frequency band at 1430 cm^{-1} for quantification of CO_2.

Since the intensity of absorbance peaks in µ-ATR spectra is highly dependent on the contact between ATR crystal and the sample, it is useful to adjust the spectra for the quality of the contact. The area of the T-O (T = Si, Al) stretching vibration band at 930 cm^{-1} (determined with a linear baseline defined by anchor points at 1200 and 790 cm^{-1}, Fig. 2) was found to be a good indicator for this contact and is therefore used for the normalization of the carbonate peak intensity. A factor of 10000 is applied to obtain convenient numbers.

This is the peer-reviewed, final accepted version for American Mineralogist, published by the Mineralogical Society of America.
The published version is subject to change. Cite as Authors (Year) Title. American Mineralogist, in press.
DOI: https://doi.org/10.2138/am-2022-8477. http://www.minsocam.org/

$$A_{norm} = 10000 * \frac{A_{1430}}{Int_{930}} \quad (1)$$

where A_{norm} is the normalized peak height of the 1430 cm^{-1} CO_3^{2-} band, A_{1430} is the baseline corrected peak height of the 1430 cm^{-1} CO_3^{2-} vibration and Int_{930} is the Integral of the baseline corrected T-O band at 930 cm^{-1}. This normalization reduces scatter in the data that result from imperfect contact between ATR crystal and the sample and therefore reduces the overall analytical error.

Our choice to use only the peak height of 1430 cm^{-1} band of the carbonate doublet for quantification has the following reasons: For low intensities, the area of broad bands such as the carbonate doublet strongly depends on the correct baseline subtraction. Furthermore, in hydrous glasses there is an overlap of the low frequency tail of the H_2O bending vibration with the high frequency tail of the carbonate doublet (Fig. 4), which would require spectral deconvolution and would introduce additional errors. In addition to that, we observe some distorted line shape of the high frequency tail of the carbonate doublet (Figs. 3 & 4). Thus, the low frequency part is at least affected, and peak heights can be determined without deconvolution. To opt for the integral of the T-O stretching band for normalization has the following reason: High concentrations of carbonate groups or dissolved water can change the degree of glass polymerization and thus the shape (width and height) of the convoluted T-O stretching band. The use of integral intensity may compensate such effects of structural changes better than the peak height. Indeed, the width of the TO band in our hydrous glasses decreases slightly with increasing water content and develops a more pronounced shoulder at the low frequency side while the peak maximum shifts from 930 cm^{-1} at 0.65 wt% H_2O to 947 cm^{-1} at 6.29 wt% H_2O (Fig. A4, electronic supplement).

Normalized µ-ATR peak heights calculated after Eq. 1 and CO_2 concentrations measured by CSA are listed in Table 2. Plotting c_{CO2} as function of A_{norm} (Fig. 5) yields a linear trend with the regression

$$c_{CO2}\ [wt\%] = 0.4394\ (\pm 0.006) * A_{norm}\ . \quad (2)$$

This is the peer-reviewed, final accepted version for American Mineralogist, published by the Mineralogical Society of America.
The published version is subject to change. Cite as Authors (Year) Title. American Mineralogist, in press.
DOI: https://doi.org/10.2138/am-2022-8477. http://www.minsocam.org/

For this dataset the estimated error for c_{CO2} from the regression (fit standard error) is 0.08 wt% (2 sigma).

Comparison between CO_2 concentrations determined by µ-ATR MIR spectroscopy and CSA shows a good agreement (Table 2). As our dataset also contains hydrous glasses with H_2O contents between 2.19 wt% and 6.29 wt% we can evaluate the influence of water on the ATR method. However, for these samples independent CO_2 measurements could not be performed with CSA due to a lack of sample material. Instead, transmission FTIR measurements were used to determine c_{CO2} of the hydrous glasses (Table 2). The data for H_2O bearing samples show a very good agreement with the data for nominally anhydrous glasses (Fig. 5), indicating that higher water contents have no influence on our ATR calibration for nominally dry glasses. This underlines the reliability of the ATR method for determination of CO_2 concentrations in leucitite glasses.

Molecular CO_2 in granitic glasses

More silicic compositions tend to incorporate CO_2 in the form of molecular CO_2 instead of or in combination with CO_3^{2-} (e.g. Brooker et al., 1999, 2001b) In transmission IR spectroscopy the v_3 anti-symmetric stretching vibration of molecular CO_2 at 2350 cm^{-1} has similar problematics as the CO_3^{2-} doublet by reaching strikingly high absorbances (Fig. 6), when CO_2 concentrations exceed 0.3 wt%, thus forcing the sample wafer thickness to be very low for the quantification of the signal.

In order to test the potential of ATR-FTIR spectroscopy to quantify molecular CO_2, we measured granitic glasses from the Okertal- and Knaupsholz granites, which contain CO_2 only in the molecular form. Carbonate groups were not detected in MIR absorption spectra measured in transmission (Fig. 6). The CO_2 contents of these glasses were determined from such absorption spectra (see Fig. A5 for the spectra of all CO_2 bearing granite glasses), using the absorption coefficient of 1214 L/mol*cm for the 2350 cm^{-1} band in rhyolite glasses from Behrens et al. (2004b). Independent CO_2

measurements with the carbon sulfur analyzer were not performed with these samples due to numerous small bubbles in major parts of the glass bodies. Water contents were determined from the absorption spectra using either the combination bands at 4500 (X-OH) and 5200 cm^{-1} (H_2O molecules) for glasses with more than 1 wt% water, or the fundamental OH stretching vibration at about 3550 cm^{-1} for low water content glasses. NIR absorption coefficients were previously determined for OTG glasses to be e_{4500}= 1.27 L/mol*cm and e_{5200}= 1.52 L/mol*cm (unpublished). For evaluation of the OH stretching vibration in the water poor glasses, the absorption coefficient e_{3600}= 75 L/mol*cm for rhyolitic glasses from Okumura et al. (2013) was used.

ATR spectra of selected granitic samples are shown in Fig. 7. Figure 7a shows an overview of the relevant spectral range for OTG-C-5KB glass with the CO_2^{mol} peak at 2350 cm^{-1} and lattice vibrations below 1300 cm^{-1} and Fig. 7b shows enlargements of the CO_2^{mol} spectral region of OTG-C-5KB, GKH-C1 and GKH-C2 glasses, which contain 0.27, 0.17 and 0.10 wt% CO_2.

Despite numerous spectral acquisitions per sample we typically obtained spectra that consisted of overlapping signals of CO_2 dissolved in the glass and atmospheric, gaseous CO_2 (Fig. 7b). The CO_2 dissolved in the glass produces a roughly Gaussian shaped absorption peak, while the signal of atmospheric CO_2 is in form of a doublet and can have either positive or negative intensities, depending on whether more or fewer CO_2 molecules were present in the beam path during single channel sample spectrum acquisition compared to the single channel reference spectrum acquisition. The doublet shape for gaseous CO_2 is the envelope of numerous, very narrow rotational vibration bands that cannot be resolved with our standard acquisition parameters for silicate glasses (spectral resolution of 4 cm^{-1}). Even with the best the spectral resolution of our instrument of 0.5 cm^{-1}, we still obtain partial overlapping of the rotational bands. The fully convolved signal from atmospheric CO_2 acquired with a spectral resolution of 4 cm^{-1} is very reproducible in terms of line shape and therefore suitable for the correction described below.

For a reliable evaluation of the μ-ATR glass spectra, the signal of the atmospheric CO_2 needs to be removed by spectral subtraction (Fig. 8). As subtrahend we collected an ATR zero-line spectrum in air, which is an ATR spectrum for which both, reference and sample single channel spectra are measured under identical acquisition conditions in air (i.e. no sample in contact with the ATR crystal). The absorbance of such zero-line spectrum should be zero over the entire spectral range. However, when the purging of the instrument is not perfect, there will be still some signal of atmospheric CO_2 and H_2O, which can have positive or negative intensities, depending on whether more or fewer CO_2 and H_2O molecules were present in the beam path during acquisition of the sample single channel spectrum with respect to the reference single channel spectrum. Before subtraction, the zero-line spectrum with a clear atmospheric CO_2 doublet must be intensity scaled to fit the glass spectrum. Therefore, a factor is applied to the zero-line spectrum until the intensity in the range 2280 to 2325 cm^{-1} fits to that of the glass spectrum, which displays a mixed signal from atmospheric and dissolved CO_2 (Fig. 8). The scaled zero-line spectrum is then subtracted from the glass spectrum leaving behind the "pure" signal from dissolved CO_2. The heights of these peaks were then normalized to the integral intensity of the T-O vibrations of the silicate network, located at 990 cm^{-1} in these glasses (baseline anchor points at 850 und 1260 cm^{-1}), and were finally multiplied by 10000 to obtain more convenient numbers. A plot of CO_2 concentrations (obtained from transmission MIR spectroscopy) versus normalized ATR intensity ($A_{norm} = A_{2350}*10000/Int_{990}$) yields an excellent linear trend passing through the origin (Fig. 9). A linear regression of the data results in the equation:

$$c_{CO2}\ [wt\%] = 0.2632\ (\pm 0.0032) * A_{norm} \quad (3)$$

with a fit standard error of about 0.005 wt% CO_2 (2 sigma).

Limitations for quantification of carbonate species

This is the peer-reviewed, final accepted version for American Mineralogist, published by the Mineralogical Society of America.
The published version is subject to change. Cite as Authors (Year) Title. American Mineralogist, in press.
DOI: https://doi.org/10.2138/am-2022-8477. http://www.minsocam.org/

In order to reliably quantify chemical components from infrared spectra, the intensities of absorption peaks must be measured with good precision and accuracy. Apart of absolute intensities, which have to lie within the linearity range of the detector, the signal to noise ratio and the reproducibility of the baseline correction are also of importance. Here we synthesized leucitite glasses with CO_2 contents down to 0.17 wt% (SULm-0.5) to demonstrate the capability of measuring low CO_2 contents. The deviation of CO_2 concentration determined by CSA and μ-ATR is quite high in this sample (12 %) as a result of the small peak height and the interference produced by atmospheric water, which gets more and more relevant during measurement of small 1430 cm^{-1} peak heights, thus reducing the signal to noise ratio.

Due to the nature of the ATR technique a certain stability of the measured samples is mandatory to realize a good contact of the Germanium crystal onto the sample. Measurements of foamy samples (e.g. pumice) may be more difficult to be realized and need good support and impregnation of the bubbles with epoxy resin. Also very thin, free standing sample wafers may break into pieces due to the force applied by the ATR crystal tip.

Since H_2O bearing samples (Fig. 4) show a H_2O vibration at ~1640 cm^{-1} (H-O-H bending) it is recommended to only use the 1430 cm^{-1} band for quantification of CO_3^{2-} in silicate glasses, as the peak height of the 1510 cm^{-1} CO_3^{2-} vibration might be slightly increased by a contribution of the H_2O vibration. Furthermore, the carbonate splitting depends on melt composition and may be as large as 300 cm^{-1}, while the midpoint of the doublet remains relatively constant between 1440 and 1490 cm^{-1} (Brooker et al., 2001b). Therefore, the overlap between the high frequency carbonate doublet peak and the H_2O bending vibration may be more severe in other glass compositions.

Even though it is possible to measure low CO_2 concentrations (down to 0.17 wt%), the ATR MIR method is most useful for silicate glasses with high CO_2 contents. This is opposite to transmission FTIR spectra that show a much higher sensitivity for CO_3^{2-} but, depending on the thickness of the

This is the peer-reviewed, final accepted version for American Mineralogist, published by the Mineralogical Society of America.
The published version is subject to change. Cite as Authors (Year) Title. American Mineralogist, in press.
DOI: https://doi.org/10.2138/am-2022-8477. http://www.minsocam.org/

406 sample quickly reaches total absorption (i.e. more than 2 AU) in samples with high CO_3^{2-} contents.
407 An advantage of μ-ATR FTIR spectra over other spectroscopic methods is the clear separation of the
408 carbonate doublet from the SiO_2 lattice vibrations allowing for a linear baseline. Transmission FTIR
409 spectra often require a more complex baseline subtraction due to the overlapping of the CO_3^{2-}
410 vibrations and silicate network vibrations (e.g. Schanofski et al., 2019). As shown by Morizet et al.
411 (2013) the quantification of CO_3^{2-} with micro-Raman spectroscopy also requires a complex spectra
412 evaluation as the T-O stretching vibrations of aluminosilicate glasses superimpose the CO_3^{2-} signal.
413

414 **Limitations for quantification of molecular CO_2**

415 Although only few glasses with dissolved molecular CO_2 were investigated in this study, the results
416 indicate that the ATR MIR method is also capable to reliably determine molecular CO_2
417 concentrations in silicate glasses above 0.1 wt%. However, as the ATR signal is weak, it may be
418 completely disguised by the signal of atmospheric CO_2. To minimize the influence of atmospheric
419 CO_2, care must be taken to keep the atmospheric conditions in the beam path of the spectrometer
420 and the microscope as constant as possible. Our Bruker™ Vertex 70 spectrometer as well as the
421 body of the Hyperion IR microscope were purged with dried and CO_2-reduced air. A long purging
422 period overnight before measuring was proven to reduce atmospheric H_2O and CO_2 signals most
423 efficiently. Furthermore, an automatic mapping of 8 or more sample spots with measuring a
424 reference spectrum every second spot and leaving the laboratory unmanned during the
425 measurements, also helped to minimize atmospheric variations during spectral acquisitions and
426 thus reduced the signal of atmospheric CO_2 in the spectra. However, as the ATR objective of our
427 Hyperion microscope is not purged nor sits in a plexiglas microscope chamber, the small variations
428 of the laboratory atmosphere still have an impact on the atmospheric H_2O and CO_2 signals of the
429 final spectrum. Thus, keeping atmospheric conditions as constant as possible is of prime importance

for a successful application of ATR IR spectroscopy for the quantitative analysis of molecular CO_2 in silicate glasses.

The ATR signal of molecular CO_2 in our granitic samples containing 0.08 to 0.27 wt% CO_2 is very small with about 0.004 to 0.013 absorbance units (Table 3), resulting in about 0.005 AU per 0.1 wt% CO_2^{mol}. This number is about 2.2 times as high as for the carbonate vibration at 1430 cm^{-1} in our leucitite glass. Considering the absorption coefficients for molecular CO_2 and carbonate groups in silicate glasses in transmission IR spectroscopy (granite: ε_{CO2mol} = 1214 L mol^{-1} cm^{-1}, Behrens et al. 2004b; leucitite: $\varepsilon_{CO3^{2-}} \approx$ 336 L mol^{-1} cm^{-1}, Schanofski et al. 2019) one could expect higher intensities of the 2350 cm^{-1} band by a factor of about 3.6. However, the sampling depth of the evanescent wave in ATR spectroscopy decreases with increasing wavenumber of the signal. At 2350 cm^{-1} the effective sampling depth is ~1.5 µm, compared to ~2.4 µm at 1430 cm^{-1} (Mirabella Jr. 1985), effectively decreasing the signal intensity of the CO_2^{mol} band by a factor of 0.63 compared to that of the CO_3^{2-} band. The combination of these approximations (2.2/0.63 ≈ 3.5 vs. 1214/336 ≈ 3.6) demonstrate the consistency of our data.

CO_2 solubility in SULm leucititic melts

The high pressure leucitite samples (P ≥ 5 kbar) synthesized in this study can complement the dataset of Schanofski et al. (2019) for the maximum solubility of CO_2 in the leucititic SULm composition at pressures above 3 kbar (Fig. 10). The samples that were synthesized using the piston cylinder apparatus were equilibrated at 1375 °C compared to 1250 °C for IHPV samples. Thibault and Holloway (1994) found a strong, negative effect of temperature on the solubility of CO_2 in another Ca-rich leucitite melt. In order to compare our datasets from different temperatures, we employed a correction to our 9 – 18 kbar samples, based on the dataset of Thibault and Holloway (1994). A constant factor of 1.159 was applied to extrapolate the experimental 1375 °C data to 1250

454 °C at constant pressure. The extrapolated data of the piston cylinder experiments are in very good
455 agreement with the CO_2 solubility below 5 kbar showing a linear increase with pressure (Fig. 10).
456 The only outlier is the data point for 9 kbar (SULm-10). In this experiment the thermocouple broke
457 at the beginning of the run during heating. The experiment was continued by adjusting the output
458 power to that of the other piston cylinder experiments and was quenched after only 30 minutes at
459 final conditions. The CO_2 concentration in SULm-10 is slightly lower than expected from the trend
460 of the other samples and may reflect uncomplete equilibration/saturation of the melt with CO_2 or
461 that the real final temperature was higher than desired.
462 In the Piston Cylinder samples SULm-20 and SULm-15s, we discovered sub-micron size quench
463 phases, which were most prominent when a low quench rate (40 °C/s vs. 120 °C/s) was used to
464 terminate the experiments. These quench phases also produced additional bands in the μ-ATR
465 spectra, which we assigned to a carbonate phase. The prominent v_3 band at about 1465 cm^{-1} points
466 towards aragonite, while the v_2 band at about 871 cm^{-1} is more consistent with calcite (Fig. 11).
467 However, as these quench crystals are too small for proper analysis with μ-ATR FTIR or Raman
468 spectroscopy, we were not able to unambiguously identify which carbonate phase crystallized
469 during quench. In extreme cases such as sample SULm-15s the v_3 vibration of the carbonate quench
470 phase is superimposed to such an extend with the glass carbonate doublet, that it is impossible to
471 evaluate the 1430 cm^{-1} band.
472
473 **Implications**
474 We introduced a new and easy to use ATR-FTIR technique for quantification of CO_2 in silicate glasses.
475 Clear linear dependences of the normalized ATR peak heights of the CO_2 related bands (carbonate
476 as well as molecular CO_2) on the CO_2 content measured by independent methods (CSA, FTIR
477 transmission spectroscopy) were found and linear correlation coefficients for the quantitative

478 determination of CO_2 concentrations in leucititic and granitic glasses were calculated. As for
479 absorption spectra measured in transmission, it is quite likely that different melt compositions
480 require individual calibrations to relate ATR intensity to concentration. This entails that for each
481 composition an independent set of calibration samples need to be prepared and to be analyzed
482 independently for CO_2. Advantages of the ATR technique over transmission FTIR spectroscopy are a
483 simplified sample preparation by requiring only one polished surface and an independence of the
484 absorbance on the sample thickness, allowing for quantification of high CO_2 concentrations. It must
485 be stated that the ATR technique measures the surface and first few µm of the sample exclusively
486 and therefore requires a clean, freshly prepared and representative sample surface to make a
487 statement for the entire sample. Compared to Raman spectroscopy, the CO_3^{2-} ATR band is much
488 less affected by signals of silicate network vibrations. As a result, a simple straight baseline can be
489 applied for the carbonate doublet in ATR FTIR spectra. Additionally, ATR FTIR signals refer to a fixed
490 sample volume that is being analyzed resulting in a good reproducibility whereas the Raman signal
491 highly depends on the focus plane.
492 Micro-ATR FTIR is a convenient technique for measuring H_2O (and now also CO_2) concentrations in
493 melt inclusions and partially crystallized samples due to the small penetration depth of the
494 evanescent wave as well as the good spatial resolution as pointed out by Lowenstern and Pitcher
495 (2013). Since the contact between sample and the Germanium crystal is crucial for the quality of
496 the spectra, we suggest normalizing the 1430 cm^{-1} CO_3^{2-} and 2350 cm^{-1} CO_2 peak heights for the
497 contact quality. As was demonstrated for our leucititic and granitic glasses, this normalization can
498 be done with the integral of T-O stretching vibrations. Such normalization is not a must, but it
499 improved the error of our datasets by 10 to 15 %. From our experience the normalization helps to
500 eliminate small outliers which may be caused by small variations in contact between ATR crystal and
501 sample. Significant outliers may be identified from the unnormalized intensities alone. The datasets

presented here do not contain such outliers as by now we gained significant experience on the importance of a clean, dust free sample surface and that the sample support should have some degree of flexibility. Embedding the sample into an epoxy pellet or placing glass slides on sticky carbon pads for SEM turned out to be a good solution. However, when we started with such ATR measurements and had less experience, we produced more outliers that could be compensated with the normalization.

Acknowledgements

This research has been partly supported by the Deutsche Forschungsgemeinschaft research Grant FA 1477/1-1. The critical comments of Giada Iacono-Marziano and 2 other anonymous reviewers as well as from the associate editor Yann Morizet greatly improved the manuscript. We also thank Yann Morizet for the editorial handling.

References

Allabar, A., and Nowak, M. (2020) High spatial resolution analysis of H_2O in silicate glass using attenuated total reflection FTIR spectroscopy coupled with a focal plane array detector. Chemical Geology, 556.

Amma, S., Kim, S.H., and Pantano, G.G. (2016) Analysis of Water and Hydroxyl Species in Soda Lime Glass Surfaces Using Attenuated Total Reflection (ATR)-IR Spectroscopy. Journal of the American Ceramic Society, 99, 128-134.

Anderson, A.T. (1975) Some basaltic and andesitic gases. Reviews of Geophysics, 13, 37-55.

Behrens, H., Ohlhorst, S., Holtz, F., and Champenois, M. (2004a) CO_2 solubility in dacitic melts equilibrated with H_2O-CO_2 fluids: Implications for modeling the solubility of CO_2 in silicic melts. Geochimica et Cosmochimica Acta, 68 (22), 4687–4703.

525 Behrens, H., Tamic, N., and Holtz, F. (2004b) Determination of the molar absorption coefficient for
526 the infrared absorption band of CO_2 in rhyolitic glasses. American Mineralogist, 89, 301-306.
527 Behrens H., Misiti V., Freda C., Vetere F., Botcharnikov R.E., and Scarlato P. (2009) Solubility of H_2O
528 and CO_2 in ultrapotassic melts at 1200 and 1250 °C and pressure from 50 to 500 MPa. American
529 Mineralogist, 94, 105-120.
530 Blank, J.G., and Brooker, R.A. (1994) Experimental studies of carbon dioxide in silicate melts:
531 Solubility, speciation, and stable carbon isotope behavior. In M.R. Carroll and J.R. Holloway,
532 Eds., Volatiles in Magmas. 30, p. 157-186. Reviews in Mineralogy Mineralogical Society of
533 America, Washington D.C.
534 Blank, J.G., Stolper, E.M., Carroll, M.R. (1993) Solubilities of carbon dioxide and water in rhyolitic
535 melt at 850 °C and 750 bars. Earth Planetary Science Letters, 119, 27–36.
536 Brooker, R.A., Kohn, S.C., Holloway, J.R., McMillan, P.F., and Carroll, M.R. (1999) Solubility,
537 speciation and dissolution mechanisms for CO_2 in melts on the $NaAlO_2$-SiO_2 join. Geochimica et
538 Cosmochimica Acta, 63, 3549-3565.
539 Brooker, R.A., Kohn, S.C., Holloway, J.R., and McMillan, P.F. (2001a) Structural controls on the
540 solubility of CO_2 in silicate melts. Part I: bulk solubility data. Chemical Geology, 174, 225-239.
541 Brooker, R.A., Kohn, S.C., Holloway, J.R., and McMillan, P.F. (2001b) Structural controls on the
542 solubility of CO_2 in silicate melts. Part II: IR characteristics of carbonate groups in silicate
543 glasses. Chemical Geology, 174, 241-254.
544 Fahrenfort, J. (1961) Attenuated total reflection. Spectrochimica Acta, 17, 698-709.
545 Fanara, S., Botcharnikov, R.E., Palladino, D.M., Adams, F., Buddensieck, J., Mulch,A., and Behrens,
546 H. (2015) Volatiles in magmas related to the Campanian Ignimbrite eruption: Experiments vs.
547 natural findings. American Mineralogist, 100, 2284–2297.

548 Fine, G., and Stolper, E. (1985) The speciation of carbon dioxide in sodium aluminosilicate glasses.
549 Contributions to Mineralogy and Petrology, 9+1, 105-121.
550 Freda, C., Gaeta, M., Giaccio, B., Marra, F., Palladino, D.M., Scarlato, P., and Sottili, G. (2011) CO_2-
551 driven large mafic explosive eruptions: the Pozzolane Rosse case study from the Colli Albani
552 Volcanic District (Italy). Bulletin of Volcanology, 73 (3), 241–256.
553 Hauri, E., Wang, J., Dixon, J.E., King, P.L., Mandeville, C., and Newman, S. (2002) SIMS analysis of
554 volatiles in silicate glasses 1. Calibration, matrix effects and comparisons with FTIR. Chemical
555 Geology, 183, 99–114.
556 Holloway, J.R., and Blank, J.G. (2004) Application of experimental results to C-O-H species in
557 natural melts. In M.R. Carroll and J.R. Holloway, Eds., Volatiles in Magmas. 30, p. 187-230.
558 Reviews in Mineralogy Mineralogical Society of America, Washington D.C.
559 Iacono-Marziano G., Morizet Y., Le Trong E., Gaillard F. (2012) New experimental data and semi-
560 empirical parameterization of H2O–CO2 solubility in mafic melts. Geochimica et Cosmochimica
561 Acta, 97, 1–23.
562 Johnson, M.C., Anderson, A.T. Jr, and Rutherford, M.J. (1994) Pre-eruptive volatile contents of
563 magmas. In M.R. Carroll and J.R. Holloway, Eds., Volatiles in Magmas. 30, p. 281-330. Reviews in
564 Mineralogy Mineralogical Society of America, Washington D.C.
565 King, P.L., Holloway, J.R. (2002) CO_2 solubility and speciation in intermediate (andesitic) melts: the
566 role of H_2O and composition. Geochimica et Cosmochimica Acta, 66, 1627–1640.
567 Lesne, P., Scaillet, B., Pichavant, M., Beny, J.-M. (2011a) The carbon dioxide solubility in alkali
568 basalts: an experimental study. Contributions to Mineralogy and Petrology, 162, 153–168.
569 Lesne, P., Scaillet, B., Pichavant, M., Iacono-Marziano, G., Beny, J.-M. (2011b) The H_2O solubility of
570 alkali basaltic melts: an experimental study. Contributions to Mineralogy and Petrology, 162,
571 133-151.

572 Li, H.H. (1993) Refractive index of silicon and germanium and its wavelength and temperature
573 derivatives, Journal of Physical and Chemical Referece Data, 9, 561-658.
574 Lowenstern, J.B., and Pitcher, B.W. (2013) Analysis of H_2O in silicate glass using attenuated total
575 reflectance (ATR) micro-FTIR spectroscopy. American Mineralogist, 98 (10), 1660–1668.
576 Mirabella Jr., F.M. (1985) Internal Reflection Spectroscopy. Applied Spectroscopy Reviews, 21 (1-
577 2), 45–178.
578 Morizet, Y., Brooker, R.A., and Kohn, S.C. (2002) CO_2 in haplo-phonolite melt: solubility, speciation
579 and carbonate complexation. Geochimica et Cosmochimica Acta, 66, 1809-1820.
580 Morizet, Y., Brooker, R.A., Iacono-Marziano, G., and Kjarsgaard, B.A. (2013) Quantification of
581 dissolved CO_2 in silicate glasses using micro-Raman spectroscopy. American Mineralogist, 98
582 (10), 1788–1802.
583 Moussallam, Y., Morizet, Y., Massuyeau, M., Laumonier, M., and Gaillard, F. (2015) CO_2 solubility in
584 kimberlite melts. Chemical Geology, 418, 198–205.
585 Mysen, B.O., Eggler, D.H., Seitz, M.G., and Holloway, J.R. (1976) Carbon dioxide in silicate melts
586 and crystals; Part I, Solubility measurements. American Journal of Science, 276 (4), 455–479.
587 Ni, H., and Keppler H. (2013) Carbon in silicate melts. In R. M. Hazen, A. P. Jones, and J. A. Baross,
588 Eds., Carbon in Earth, Reviews in Mineralogy & Geochemistry, 75, 251-287, Mineralogical
589 Society of America, Chantilly, USA.
590 Okumura, S., Nakamura, M., and Nakashima, S. (2003) Determination of molar absorptivity of IR
591 fundamental OH-stretching vibration in rhyolitic glasses. American Mineralogist, 88 (11-12),
592 1657-1662.
593 Pan, V., Holloway, J.R., and Hervig, R.L. (1991) The pressure and temperature dependence of
594 carbon dioxide solubility in tholeiitic basalt melts. Geochimica et Cosmochimica Acta, 55 (6),
595 1587–1595.

Pollack, J.B., Toon, O.B., and Khare, B.N. (1973) Optical properties of some terrestrial rocks and glasses. Icarus, 19, 372-389.

Schanofski, M., Fanara, S., Schmidt, B.C. (2019) CO_2–H_2O solubility in K-rich phonolitic and leucititic melts. Contributions to Mineralogy and Petrology, 174 (6).

Shishkina, T.A., Botcharnikov, R.E., Holtz, F., Almeev, R.R., Jazwa, A.M., Jakubiak, A.A. (2014) Compositional and pressure effects on the solubility of H_2O and CO_2 in mafic melts. Chemical Geology 388, 112–129.

Stalder, R. (2004) Influence of Fe, Cr and Al on hydrogen incorporation in orthopyroxene. European Journal of Mineralogy, 16 (5), 703-711.

Symonds, R.B., Rose, W.I., Bluth, G.J.S., and Gerlach T.M. (1994) Volcanic-gas studies: Methods, results, and applications. In M.R. Carroll, and J.R. Holloway, Eds., Volatiles in Magmas, 30, p. 1-66. Reviews in Mineralogy, Mineralogical Society of America, Washington D.C.

Thibault, Y., and Holloway, J.R. (1994) Solubility of CO_2 in a Ca-rich leucitite: effects of pressure, temperature, and oxygen fugacity. Contributions to Mineralogy and Petrology, 116 (1-2), 216–224.

Figure captions

Fig. 1: FTIR MIR absorption spectrum measured in transmission of the sample SULm_3_1. The CO_3^{2-} doublet of the spectrum shows absorbances above the detector linearity limit at a thickness

of 122 µm. A sample thickness of ~ 60 µm would be required to quantify the CO_2 content. For samples of higher CO_2 content this problem intensifies (e.g. 15 µm for 4 wt% CO_2). The spectrum does not contain a signal from molecular CO_2, which would be a narrow peak at 2350 cm^{-1}.

Fig. 2: ATR FTIR spectrum of the sample SULm_15. Dashed lines are baselines applied for determination of the CO_3^{2-} peak height at 1430 cm^{-1} and the integral of the T-O stretching vibration at 930 cm^{-1}. The integral of the T-O band (Int_{930}) is used normalize the spectrum for the quality of the contact between the ATR crystal and the sample (Eq. 1).

Fig. 3: µ-ATR FTIR spectra of all nominally dry leucitite (SULm) samples (0.35 – 0.65 wt% H_2O, measured by FTIR) with (A) CO_2 contents from ATR measurements below 1 wt% (A) and above 1 wt% (B). Legends and spectra are organized in the same order. Spectra are normalized for Int_{930} and shifted in y-direction for better visibility. The enhanced spectral noise in the range of about 1850 to 1450 cm^{-1} is due to rotational-vibrational transitions of the bending mode of atmospheric H_2O molecules in the beam path.

Fig. 4: ATR FTIR spectra for H_2O bearing leucitite samples (SULm_3_5 and SULm_3_3) in comparison to the nominally dry sample SULm_3_1 on the very bottom. Spectra are normalized to Int_{930} and shifted in y-direction for better visibility. The enhanced spectral noise in the range of about 1850 to 1450 cm^{-1} is due to rotational-vibrational transitions of the bending mode of atmospheric H_2O molecules in the beam path. In water bearing glasses a signal due to H_2O bending vibrations develops at 1640 cm^{-1}, partly overlapping with the high frequency band of the carbonate doublet.

644

645

646 Fig. 5: CO_2 content measured by CSA vs. normalized peak height A_{norm} for all samples of the SULm
647 composition. Error bars represent the error propagation of 2σ errors of A_{1430} and Int_{930} parallel to
648 the y-axis and the 2σ error of repeated CSA measurements of each sample parallel to the x-axis.
649 Solid, straight line represents the linear regression forced through the zero intercept. The slope of
650 the regression is the correlation coefficient.

651

652

653 Fig. 6: MIR transmission spectra of OTG-C-5KB (upper spectrum) and a CO_2 free OTG glass (lower
654 spectrum), doubly polished to a thickness of 102 and 100 µm, respectively. The two spectra are
655 separated in intensity for better visibility. The absorption peak of the v3 asymmetric stretching
656 vibration of CO_2^{mol} at 2350 cm^{-1} in OTG-C-5KB has a peak height of about 1.8 absorption units and
657 approaches the linearity limit of the detector. The small peak at 2283 cm^{-1} is the v3 band of $^{13}CO_2$
658 and the broad, asymmetric peak at 3600 cm^{-1} is the fundamental stretching vibration of O-H groups.
659 The peaks and shoulders in the range 2100 to 1500 cm^{-1} are the result of overlapping overtones and
660 combination bands of lattice vibrations from the aluminosilicate network, and appear in exactly the
661 same way as in CO_2 free OTG glasses, indicating that CO_2 bearing OTG glass does not contain
662 carbonate groups. The strong intensity increase at about 1400 cm^{-1} is the high frequency flank of
663 the T-O stretching vibration of tetrahedrally coordinated network formers.

664

665

666 Fig. 7: ATR FTIR spectra of selected granitic samples. (A) Spectrum of OTG-C-5KB in the range from
667 2800 to 600 cm^{-1}, showing the CO_2^{mol} peak at 2350 cm^{-1} and lattice vibrations below 1300 cm^{-1}. The

668 baseline used for the integration of the 990 cm^{-1} band for the intensity normalization of the CO_2^{mol}
669 band is shown as dashed line. (B) Enlargement of the CO_2^{mol} spectral region of OTG-C-5KB, GKH-C1
670 and GKH-C2 glasses from top to bottom for demonstration of the effect of atmospheric CO_2 on the
671 spectra. Two spectra are shown for all 3 glasses and all spectra are shifted in y-direction for better
672 visibility. The top spectrum for each glass is only slightly affected by the signal of atmospheric CO_2
673 while the bottom spectrum is moderately affected by atmospheric CO_2. In the cases shown, the
674 positive peak of dissolved CO_2 is overlapping with a negative doublet of atmospheric CO_2, which
675 results from slightly higher CO_2 concentration in the beam path during acquisition of the reference
676 single channel spectrum compared to the sample single channel spectrum.
677
678
679 Fig. 8: Removal of the signal from atmospheric CO_2 by spectral subtraction. The red spectrum at the
680 bottom corresponds to the original glass spectrum (GKH-1C) with overlap of dissolved CO_2 with a
681 negative doublet of atmospheric CO_2. The top spectrum (ZERO untreated) is a zero-line spectrum,
682 derived by measuring both, reference and sample single channel spectrum of air (no sample). The
683 positive intensity of the atmospheric CO_2 doublet indicates a higher CO_2 concentration in the beam
684 path during sample single channel spectrum acquisition. This zero-line spectrum is scaled to the
685 glass spectrum, such that the flanks of the atmospheric CO_2 doublet fit the shape of the glass
686 spectrum (ZERO scaled). The scaled zero-line spectrum is subtracted from the glass spectrum
687 resulting in a spectrum that is free of the signal from atmospheric CO_2 (GKH-1C atmCO2subt) in the
688 middle. Spectra are shifted in y-direction for better visibility.
689
690

This is the peer-reviewed, final accepted version for American Mineralogist, published by the Mineralogical Society of America.
The published version is subject to change. Cite as Authors (Year) Title. American Mineralogist, in press.
DOI: https://doi.org/10.2138/am-2022-8477. http://www.minsocam.org/

Fig. 9: Correlation between CO_2^{mol} concentration derived from MIR transmission measurements and MIR ATR intensity of the 2350 cm^{-1} peak (peak height) normalized to the integral intensity of the T-O stretching vibration at 990 cm^{-1} (similar procedure as for the leucitite glasses). The data define a clear linear correlation, which can be regressed by a straight line with the y-intercept at zero

Fig. 10: CO_2 solubility as a function of pressure for all nominally dry (0.35 – 0.65 wt% H_2O) leucitite samples of the SULm composition. Grey data points are samples synthesized in the IHPV at 1250 °C. Errors are within the symbol size. White datapoints are samples synthesized in the Piston Cylinder Apparatus at 1375 °C. The CO_2 solubility of the samples synthesized at 1375 °C was extrapolated to 1250 °C for comparison (see text for details). Solid straight line represents the linear regression of all datapoints (with exception of SULm-10 due to thermocouple failure during the experiment) and demonstrates the linear dependence of the CO_2 solubility on pressure.

Fig. 11: ATR FTIR spectra of samples SULm-15s and SULM-20 containing carbonate quench crystals. A scaled spectrum of Aragonite (Ara) and Calcite (CC) powder measured with a diamond ATR-unit (Bruker™ Platinum ATR) is shown for comparison. Spectra are shifted in y-direction for better visibility.

Fig. A1: Determination of the linearity limit of the MCT detector of the Bruker™ Hyperion 3000 microscope at the Geoscience Center Göttingen. (A) Transmission FT-IR measurements of 1 to 8 layers of 1.5 µm thin Mylar foils (Fluxana™ Mylar X-ray film sheets TF-115-345) with increasing

715 cumulative thickness. Up to 8 layers the peak height of the 1342 cm^{-1} band increases linearly up to
716 1.95 absorbance units without deviation from the linear trend, indicating that linearity limit is not
717 yet reached. (B -D) Transmission FT-IR measurements of doubly polished sections of polystyrene
718 hard plastics. The evaluation of the peak heights of the absorption bands at 1747, 1872 and 1943
719 cm^{-1} as function of sample thickness indicates a deviation from the linear trend above 2.2
720 absorbance, indicating that the MCT detector has a linear response between 0 and at least 2
721 absorbance units.
722
723
724 Fig. A2: Trends of the signal intensities of (A) the 1430 cm^{-1} band (peak height) (B) the 930 cm^{-1} band
725 (integral) and (C) normalized carbonate intensity (A_{norm}) as function of the force level of the ATR
726 crystal on the sample (SULm_10). Data points are the average of 4 measurements and the error bars
727 correspond to their standard deviations (1σ). The sampling position is identical for all
728 measurements. At level 3, the unnormalized intensities reach nearly constant values (A, B),
729 indicating that optimum contact between ATR crystal and sample is reached. The normalized
730 intensities A_{norm} lie within error for force levels 2 to 5 (C), indicating that the normalization can
731 compensate at least those differences in contact that would correspond to a force level of 3 ± 1. If
732 the contact force is too low (e.g. force level 1) the normalization is not capable to fully compensate
733 the weaker contact.
734
735
736 Fig. A3: MIR transmission spectra of nominally dry leucititic samples with decreasing CO_2 content
737 from top to bottom (0.84 wt% – 0.15 wt%). Spectra were normalized to a thickness of 100 µm and
738 shifted in y-direction to improve visibility. The sharp peak on top of the 1510 cm^{-1} carbonate band

739 of SULm_3_1 is a spectral artefact caused by nearly total absorption in this spectral region for the
740 sample thickness (original thickness of the measured wafer was 122 µm).
741
742
743 Fig. A4: ATR FTIR spectra of SULm glasses synthesized at 3 kbar with decreasing H_2O content from
744 top to bottom (6.29 wt% to 0.65 wt%). Whilst the shape of the lattice vibration band at roughly 930
745 cm^{-1} is unchanged by the presence of water, the peak position is shifting towards higher
746 wavenumbers with increasing H_2O content.
747
748
749 Fig. A5: MIR transmission spectra of granitic samples with decreasing CO_2 content from top to
750 bottom (0.27 wt% – 0.08 wt%). Spectra were normalized to a thickness of 100 µm and are shifted in
751 y-direction to improve visibility. For the water rich samples with more than 2.3 wt% water (GKH-
752 HC2, GKH-HC1), the fundamental OH stretching vibration at about 3550 cm^{-1} shows total absorption
753 and for GKH-C2 (1.17 wt% water) this band exceeds the linearity limit of 2 absorbance units of the
754 detector (note that the original sample thickness was 212 µm). All three hydrous glass transmission
755 spectra display a band at about 1635 cm^{-1}, which is due to the bending vibration of H_2O molecules.
756 The sharp peak at 2350 cm^{-1} is the v3 asymmetric stretching vibration of CO_2 molecules. No
757 carbonate signal is visible in these spectra, which is expected to give rise to a doublet in the range
758 of 1350 to 1650 cm^{-1} (Brooker et al., 1999).
759

Table 1
Glass compositions measured by micro-XRF analyses.

	SiO_2	TiO_2	Al_2O_3	Fe_2O_3	MnO	MgO	CaO	Na_2O	K_2O	P_2O_5	total
SULm	44.75 (15)	0.97 (1)	16.63 (13)	10.77 (7)	0.27 (1)	4.03 (12)	10.97 (5)	2.50 (21)	9.11 (4)		100
GKH	75.10 (21)	0.23 (1)	13.11 (9)	1.78 (3)	0.04 (1)	0.33 (6)	0.87 (2)	2.89 (23)	5.63 (4)	0.03 (2)	100
OTG	76.35 (25)	0.19 (1)	12.82 (9)	1.53 (3)	0.03 (1)	0.32 (6)	0.29 (1)	2.93 (29)	5.51 (5)	0.03 (3)	100

Notes: Micro-XRF analyses are based on 20 measurements on a large fragment of the glass
Element concentrations obtained by the standardless μ-XRF analysis were corrected using a set of about 50 natural and synthetic aluminosilicate glasses with knowr
All values show content in wt%
2σ (last decimals) is given in parentheses
All iron is given as Fe_2O_3

Table 2 - Experimental conditions and volatile contents of the leucitite samples

Sample	Glaspowder [mg]	$Ag_2C_2O_4$ [mg]	H_2O [mg]	Duration [h]	Pressure [kbar]	Temperature [°C]	H_2O (IR) [wt%]	[a]A_{1430}(trans)	thickness [µm]	density [g/L]	[b] cCO_2 (trans) [wt%]	[a]A_{1430}	[a]Int_{930}	[a]A_{norm}	CO_2 (ATR) [wt%]	CO_2 (CSA) [wt%]
SULm_0.5_1	201.1	54.6		71	0.5	1250	0.35 (2)	0.346 (39)	115 (5)	2703 (24)	0.15 (2)	0.0039 (6)	100.89 (0.13)	0.383 (61)	0.17 (3)	0.15 (1)
SULm_1_1	202.4	54.7		72	1.0	1250	0.47 (5)	0.934 (38)	135 (4)	2704 (12)	0.33 (2)	0.0069 (0)	98.07 (2.30)	0.704 (17)	0.31 (1)	0.31 (3)
SULm_1.5_1	201.6	54.5		44	1.5	1250	0.36 (2)	0.884 (17)	107 (1)	2706 (14)	0.40 (2)	0.0086 (6)	94.46 (4.60)	0.914 (24)	0.40 (1)	0.40 (1)
SULm_2_1	202.1	55.7		47	2.0	1250	0.50 (3)	1.286 (79)	111 (8)	2712 (15)	0.56 (6)	0.0134 (6)	99.10 (0.08)	1.349 (61)	0.59 (3)	0.54 (2)
SULm_2.5_1	201.9	57.0		17	2.5	1250	0.37 (12)	1.461 (46)	115 (2)	2718 (11)	0.61 (4)	0.0148 (5)	98.54 (0.09)	1.505 (46)	0.66 (2)	0.64 (5)
SULm_3_1	200.6	58.0		76	3.0	1250	0.65 (3)	n.d.	122 (5)	n.d.	n.d.	0.0200 (2)	99.29 (0.35)	2.011 (18)	0.88 (1)	0.84 (6)
SULm_5_1	200.1	26.5		93	5.0	1250	n.d.	n.d.	n.d.	n.d.	n.d.	0.0259 (2)	92.77 (0.44)	2.796 (16)	1.23 (1)	1.14 (8)
[c,d]SULm_10	70.2	10.8		0.5	9.0	1375	n.d.	n.d.	n.d.	n.d.	n.d.	0.0388 (20)	96.30 (0.29)	4.025 (217)	1.77 (10)	1.82 (6)
[d]SULm_15	76.6	23.5		18.5	13.5	1375	n.d.	n.d.	n.d.	n.d.	n.d.	0.0695 (11)	99.21 (0.26)	7.010 (95)	3.07 (5)	3.11 (12)
[d,e]SULm_20	70.0	27.0		22.5	18.0	1375	n.d.	n.d.	n.d.	n.d.	n.d.	0.0929 (104)	95.47 (6.57)	9.728 (425)	4.27 (19)	4.28 (14)
SULm_3_2	198.6	51.9	4.2	76	3.0	1250	2.19 (25)	1.290 (3)	77 (3)	2689 (14)	0.82 (5)	0.0174 (3)	95.99 (1.92)	1.813 (7)	0.80 (1)	n.d.
SULm_3_3	203.2	46.3	8.6	76	3.0	1250	3.58 (16)	1.123 (2)	79 (3)	2667 (11)	0.70 (4)	0.0154 (2)	98.43 (0.08)	1.568 (38)	0.69 (1)	n.d.
SULm_3_4	199.9	34.6	14.1	76	3.0	1250	4.75 (40)	0.913 (5)	77 (3)	2671 (12)	0.58 (4)	0.0137 (5)	97.95 (1.17)	1.399 (40)	0.61 (2)	n.d.
SULm_3_5	201.9	19.8	20.6	76	3.0	1250	6.29 (45)	0.520 (5)	73 (3)	2644 (7)	0.35 (2)	0.0087 (3)	98.33 (0.22)	0.881 (22)	0.39 (1)	n.d.
[d,e,f]SULm_15s	69.9	17.1		18	13.5	1375	n.d.					n.d.	n.d.	n.d.	n.d.	n.d.

Notes: A_{1430}= Peak height of the 1430 cm^{-1} carbonate band; Int_{930}= Integral of the 930 cm^{-1} T-O band; A_{norm}= normalized peak height ot the 1430 cm^{-1} carbonate band

$_{5200}$= 1.00 L/mol*cm; $_{4500}$= 0.42 L/mol*cm from Schanofski et al. (2019) were used for NIR H_2O determination of SULm samples.

2σ error (last decimals) is given in parentheses for H_2O and CO_2 values

[a] Average value of three measurements

[b] determined by transmission FTIR using ε_{1430}=336 L/mol*cm from Schanofski et al. (2019)

[c] experimental temperature uncertain due to thermocouple failure. Experiment was performed with the same output power as the other piston cylinder runs

[d] Pressure in Piston Cylinder experiments was corrected for 10 % friction

[e] sub micron Aragonite quench phase detected

[f] sample with slow quench (40°C/s)

Standard deviations (2 sigma) and propagated errors are given as last decimals in parentheses

n.d. not determined

Table 3 - Experimental conditions and volatile contents of the granite samples

Sample	CO_2 source	Glaspowder [mg]	CO_2 source [mg]	Duration [h]	Pressure [kbar]	Temperature [°C]	[a] H_2O (IR) [wt%]	[b] A_{2350} (trans)	c thickness [µm]	[d] cCO_2 (trans) [wt%]	[e] A_{2350} (ATR)	[f] Int_{990} (ATR)	[g] A_{norm}(ATR)	[h] cCO_2 (ATR) [wt%]
GKH-HC2	$H_2C_2O_4 * 2H_2O$	255.6	26.2	136	2.0	1200	2.62 (NIR)	1.120 (10)	211 (4)	0.083 (6)	0.0041 (9)	128.97 (5.67)	0.3184 (539)	0.084 (16)
GKH-C2	$Ag_2C_2O_4$	240.1	9.6	136	2.0	1200	1.17 (NIR)	1.316 (15)	212 (4)	0.097 (7)	0.0049 (5)	131.98 (0.27)	0.3719 (380)	0.098 (11)
GKH-HC1	$H_2C_2O_4 * 2H_2O$	213.1	22.9	116	3.0	1105	2.36 (NIR)	1.596 (22)	165 (5)	0.151 (11)	0.0077 (5)	132.22 (0.57)	0.5830 (344)	0.153 (10)
GKH-C1	$Ag_2C_2O_4$	209.4	11.8	116	3.0	1105	0.17 (MIR)	1.693 (107)	157 (6)	0.168 (16)	0.0086 (6)	133.54 (0.92)	0.6459 (388)	0.170 (11)
OTG-C-5KB	$Ag_2C_2O_4$	241.5	6.2	93	5.0	1250	0.19 (MIR)	1.766 (50)	102 (4)	0.270 (22)	0.0134 (8)	132.01 (0.84)	1.0143 (574)	0.267 (16)

Notes:

[a] Water contents measured by IR transmission spectroscopy using NIR absorption coefficients e5200= 1.52 and e4500= 1.27 L/mol*cm determined for OTG glasses or using the MIR absorption coefficient e3600 = 75 L/mol*cm from Okumura et al. (2003)

[b] Peak height of the 2350 cm-1 CO_2 stretching vibration, average value of 3-5 MIR transmission measurements

[c] Thickness measured with a digital Mitutoyo micrometer gauge, the error is calculated from the measured variation in thickness and the absolute error of the gauge (±3 µm)

[d] determined using e2350= 1214 L/mol*cm from Behrens et al. (2004b) and a glas density of 2325 ± 25 g/L

[e] Peak height of the 2350 cm-1 CO_2 stretching vibration in MIR ATR spectra, average value of 8-12 ATR measurements

[f] Integral of the T-O stretching vibration in the range 850-1260 cm^{-1}, average value of 8-12 ATR measurements

[g] Anorm = A2350 (ATR) * 10000 / Int990 (ATR), average value of 8-12 ATR measurements

[h] calculated with the regression y = 0.2631(±0.0032) * A^{norm}(ATR)

Standard deviations (2 sigma) and propagated errors are given as last decimals in parentheses

Fig.1

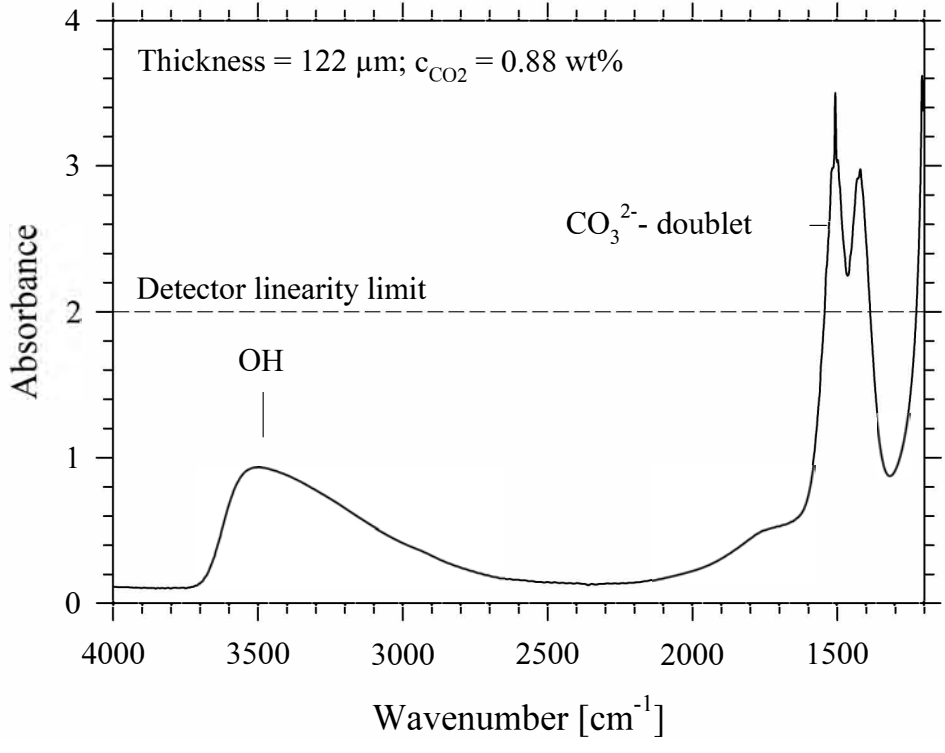
Thickness = 122 μm; c_{CO2} = 0.88 wt%
CO_3^{2-}- doublet
Detector linearity limit
OH
Absorbance
Wavenumber [cm^{-1}]
0
1
2
3
4
4000
3500
3000
2500
2000
1500

Fig. 2

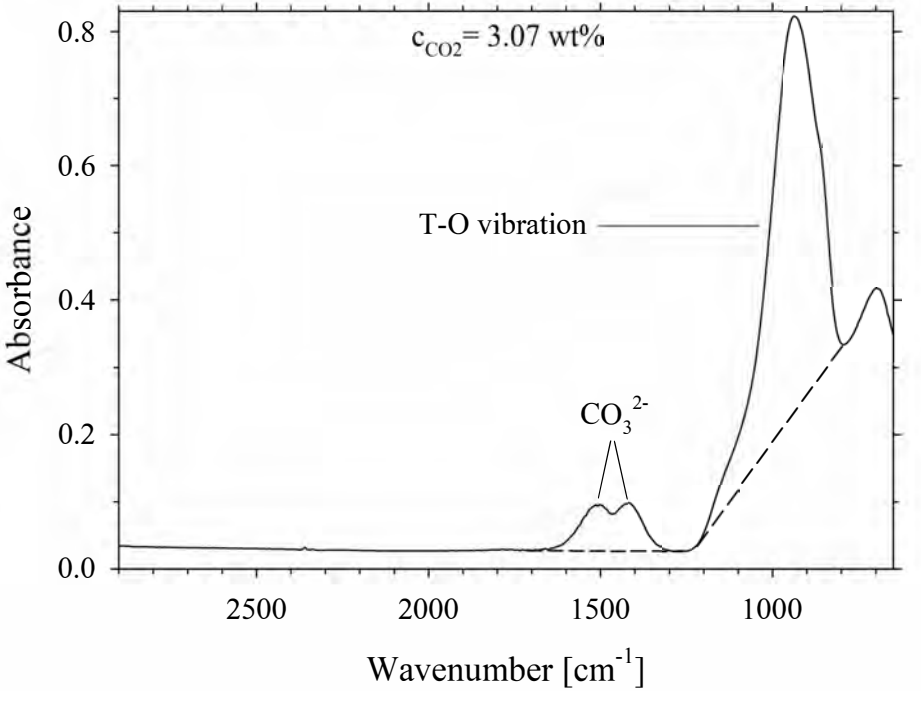
c_{CO2}= 3.07 wt%
T-O vibration
CO_3^{2-}
Absorbance
0.0
0.2
0.4
0.6
0.8
2500
2000
1500
1000
Wavenumber [cm^{-1}]

Fig. 3a

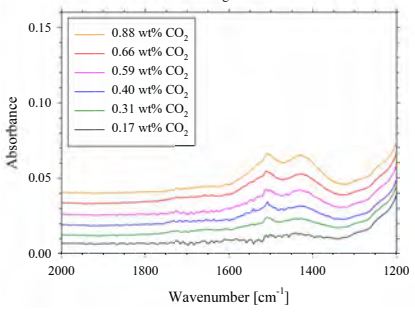
0.88 wt% CO_2
0.66 wt% CO_2
0.59 wt% CO_2
0.40 wt% CO_2
0.31 wt% CO_2
0.17 wt% CO_2
Absorbance
0.15
0.10
0.05
0.00
2000
1800
1600
1400
1200
Wavenumber [cm^{-1}]

Fig. 3b

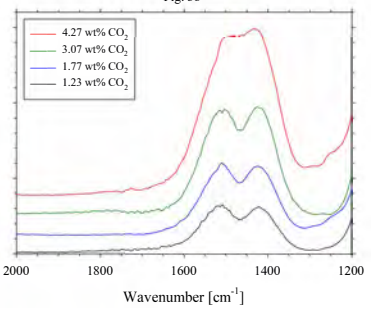
4.27 wt% CO_2
3.07 wt% CO_2
1.77 wt% CO_2
1.23 wt% CO_2
2000
1800
1600
1400
1200
Wavenumber [cm^{-1}]

Fig. 4

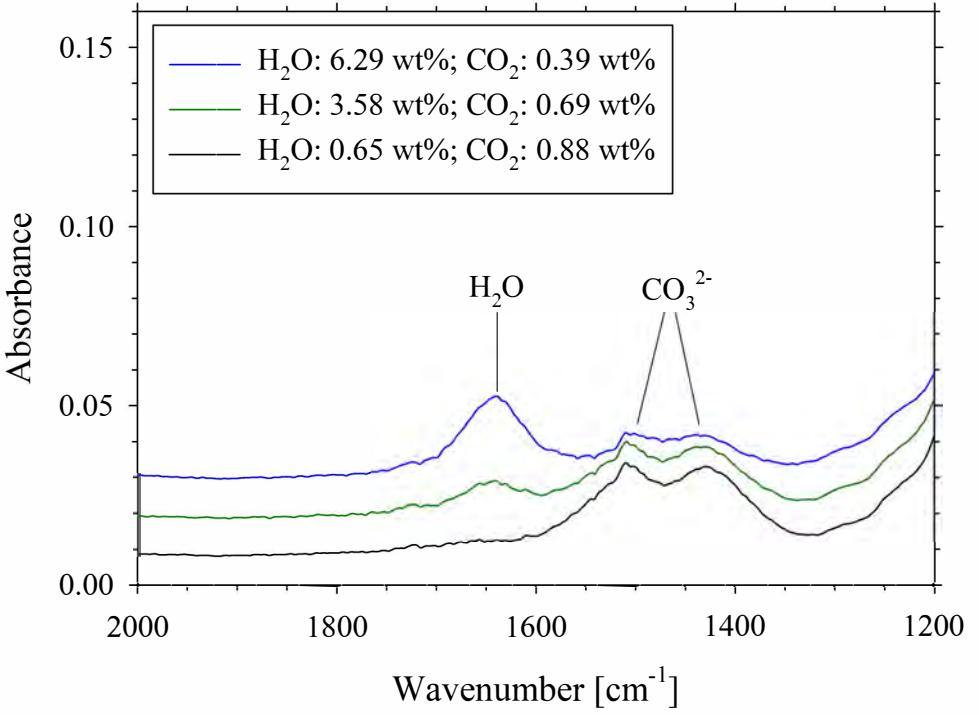
H2O: 6.29 wt%; CO2: 0.39 wt%
H2O: 3.58 wt%; CO2: 0.69 wt%
H2O: 0.65 wt%; CO2: 0.88 wt%
H2O
CO3 2-
Absorbance
0.15
0.10
0.05
0.00
2000
1800
1600
1400
1200
Wavenumber [cm-1]

Fig. 5

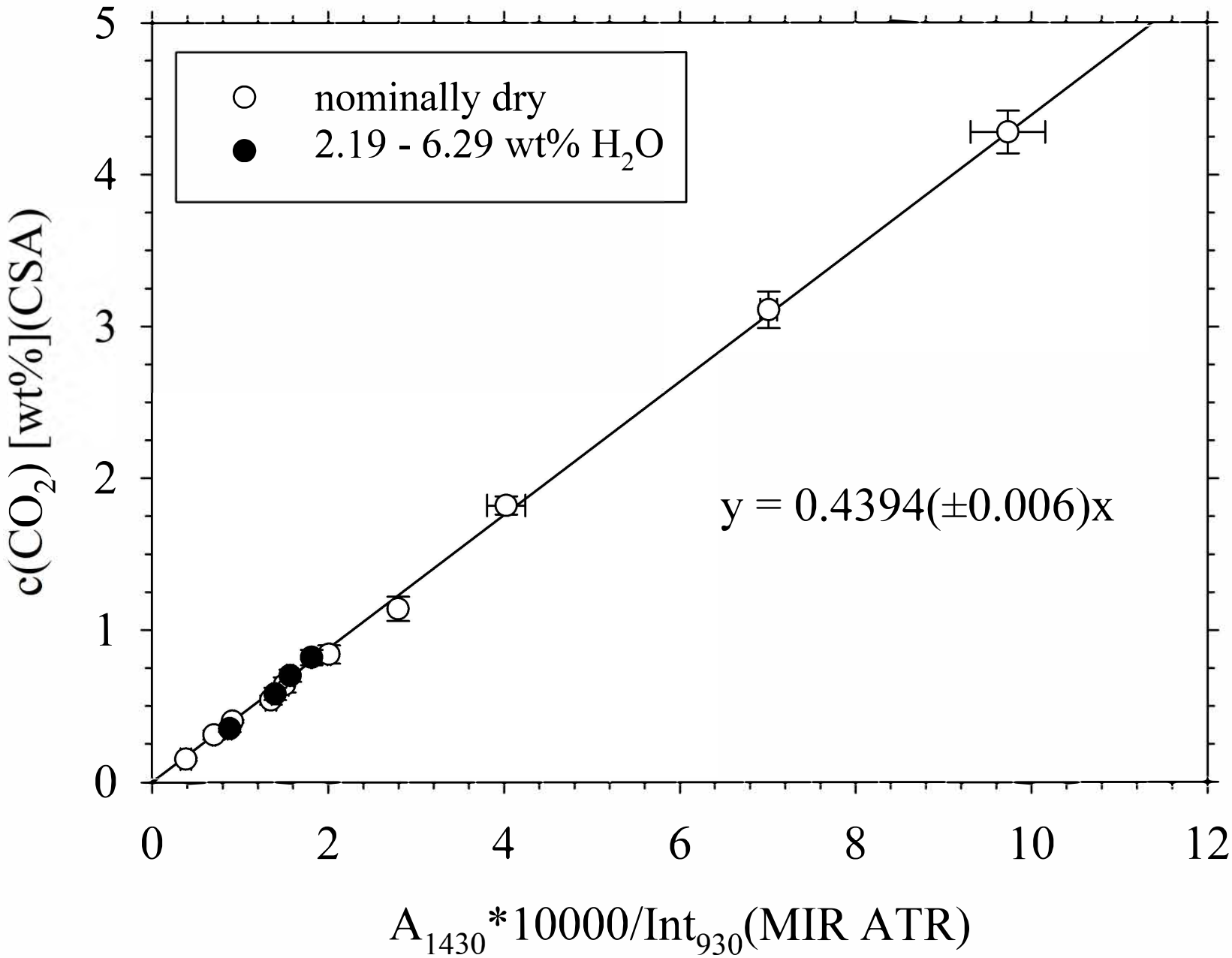
nominally dry
2.19 - 6.29 wt% H2O
y = 0.4394(±0.006)x
c(CO2) [wt%](CSA)
A1430*10000/Int930(MIR ATR)
0
1
2
3
4
5
0
2
4
6
8
10
12

Fig. 6

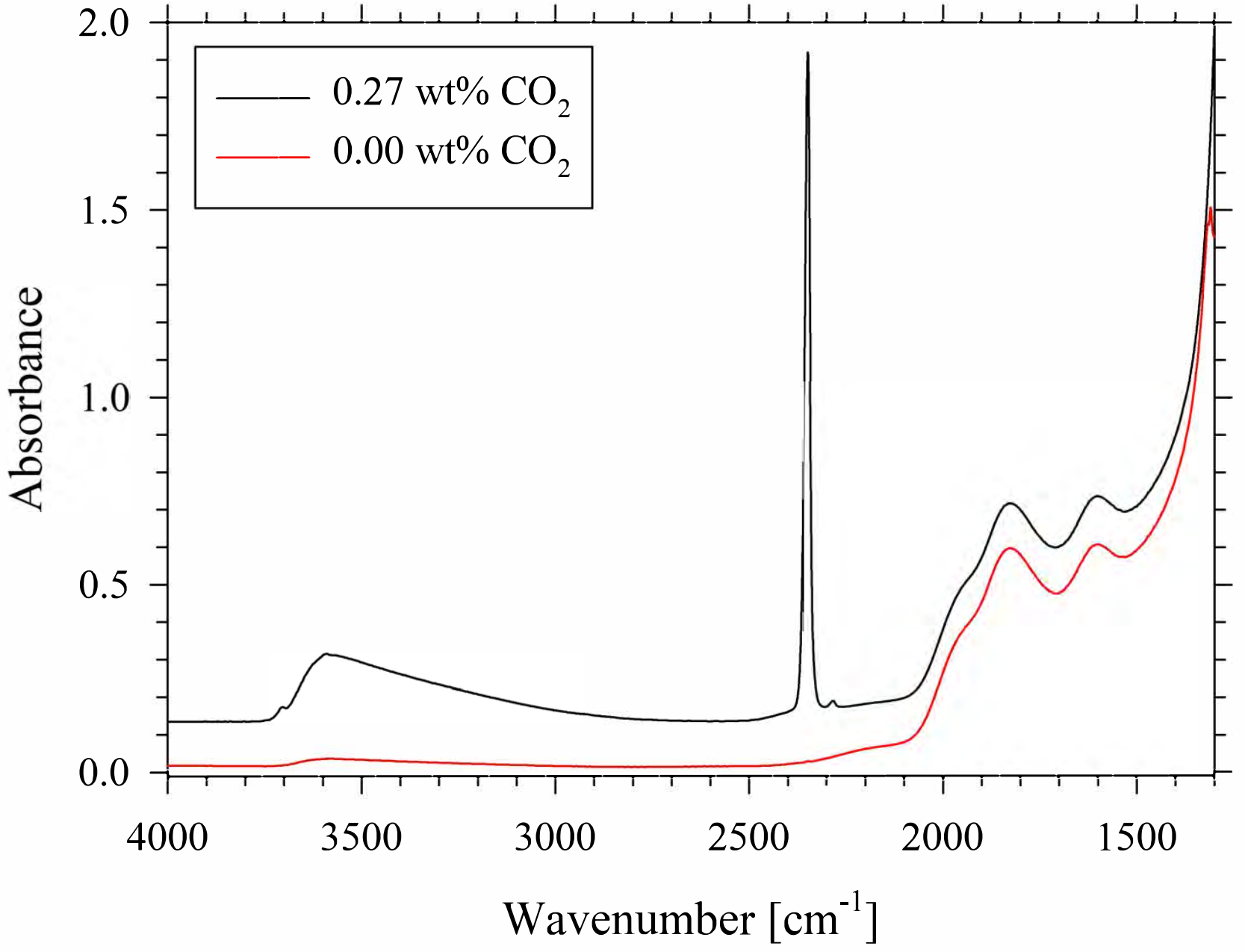
0.27 wt% CO2
0.00 wt% CO2
Absorbance
2.0
1.5
1.0
0.5
0.0
4000
3500
3000
2500
2000
1500
Wavenumber [cm-1]

Fig. 7a

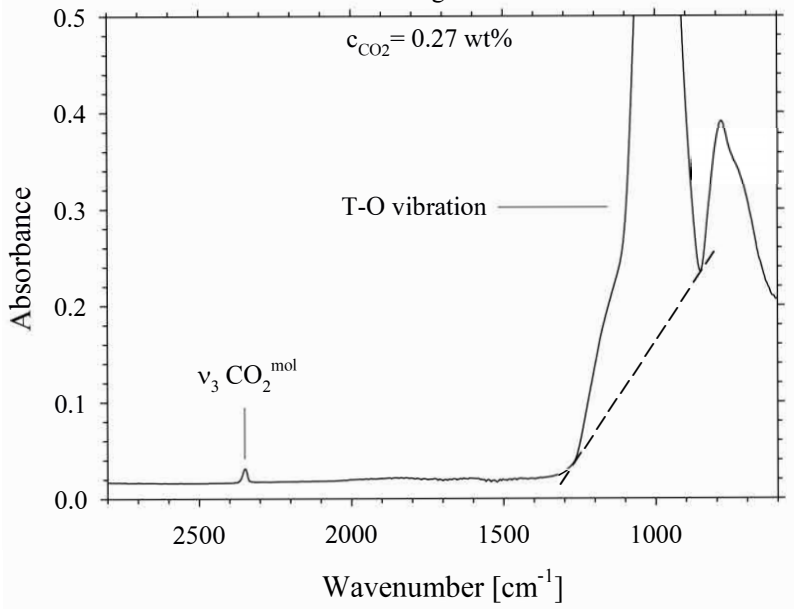
c_{CO2}= 0.27 wt%
T-O vibration
ν_3 CO_2^{mol}
Absorbance
Wavenumber [cm^{-1}]
0.0
0.1
0.2
0.3
0.4
0.5
2500
2000
1500
1000

Fig. 7b

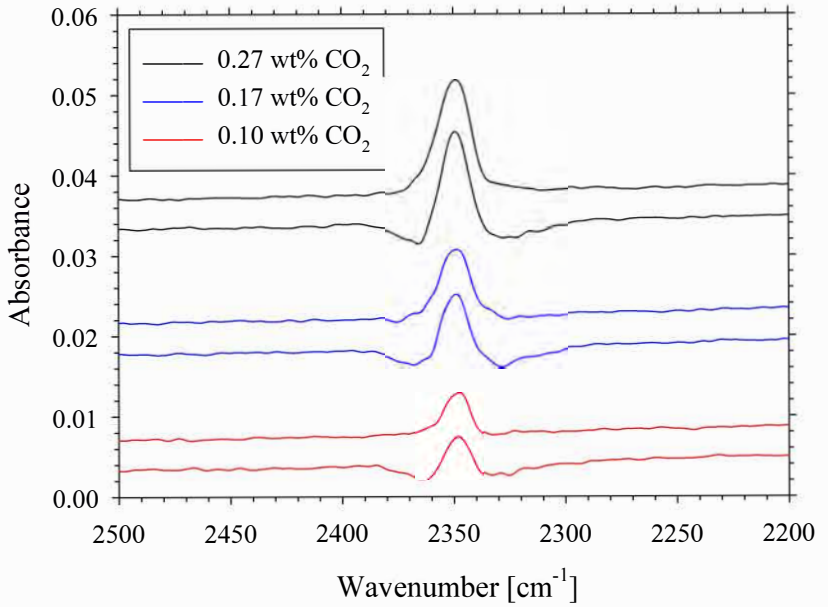
0.27 wt% CO_2
0.17 wt% CO_2
0.10 wt% CO_2
Absorbance
Wavenumber [cm^{-1}]
0.00
0.01
0.02
0.03
0.04
0.05
0.06
2500
2450
2400
2350
2300
2250
2200

Fig. 8

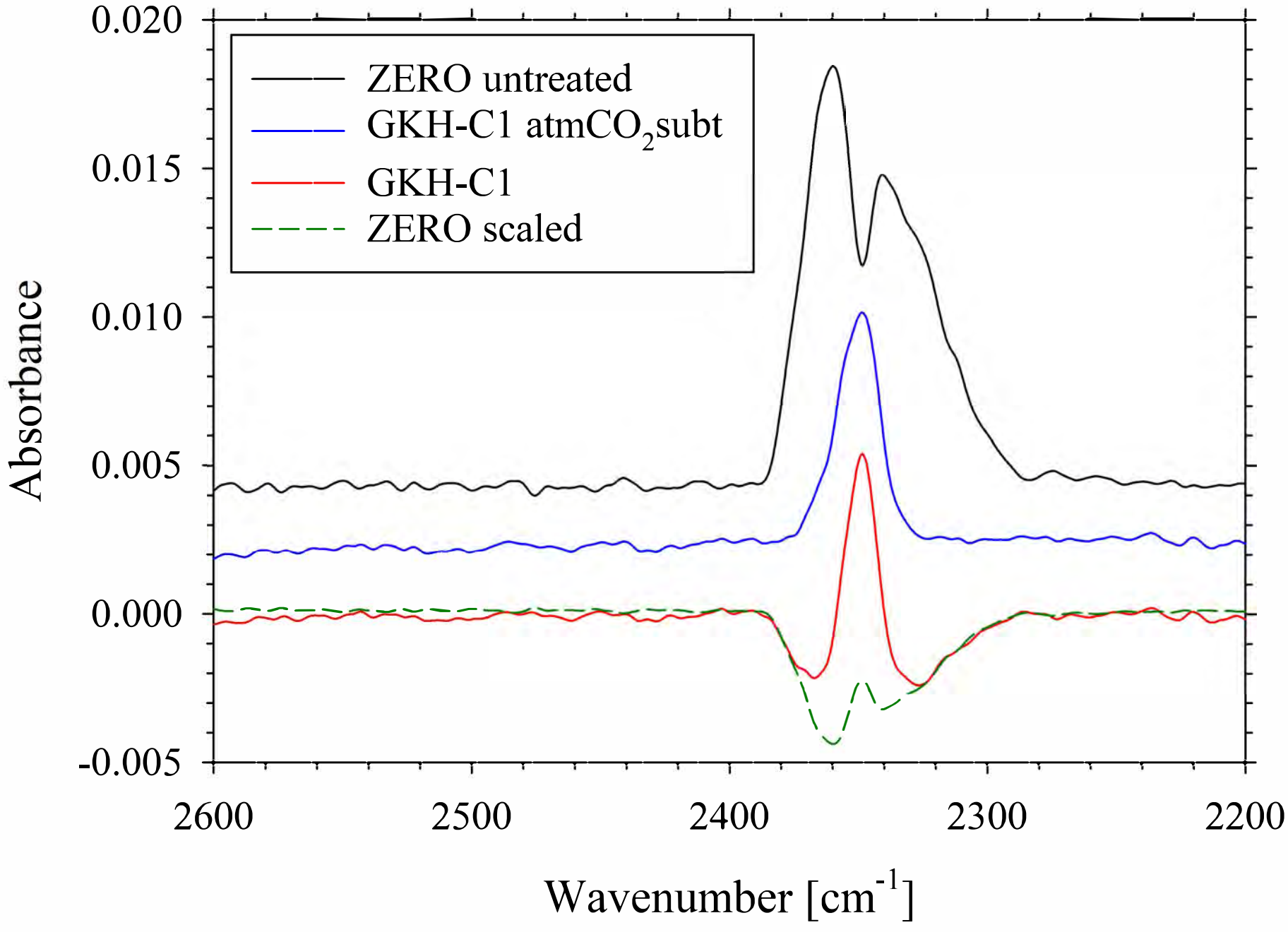
0.020
0.015
0.010
0.005
0.000
-0.005
Absorbance
2600
2500
2400
2300
2200
Wavenumber [cm-1]
ZERO untreated
GKH-C1 atmCO2subt
GKH-C1
ZERO scaled

Fig. 9

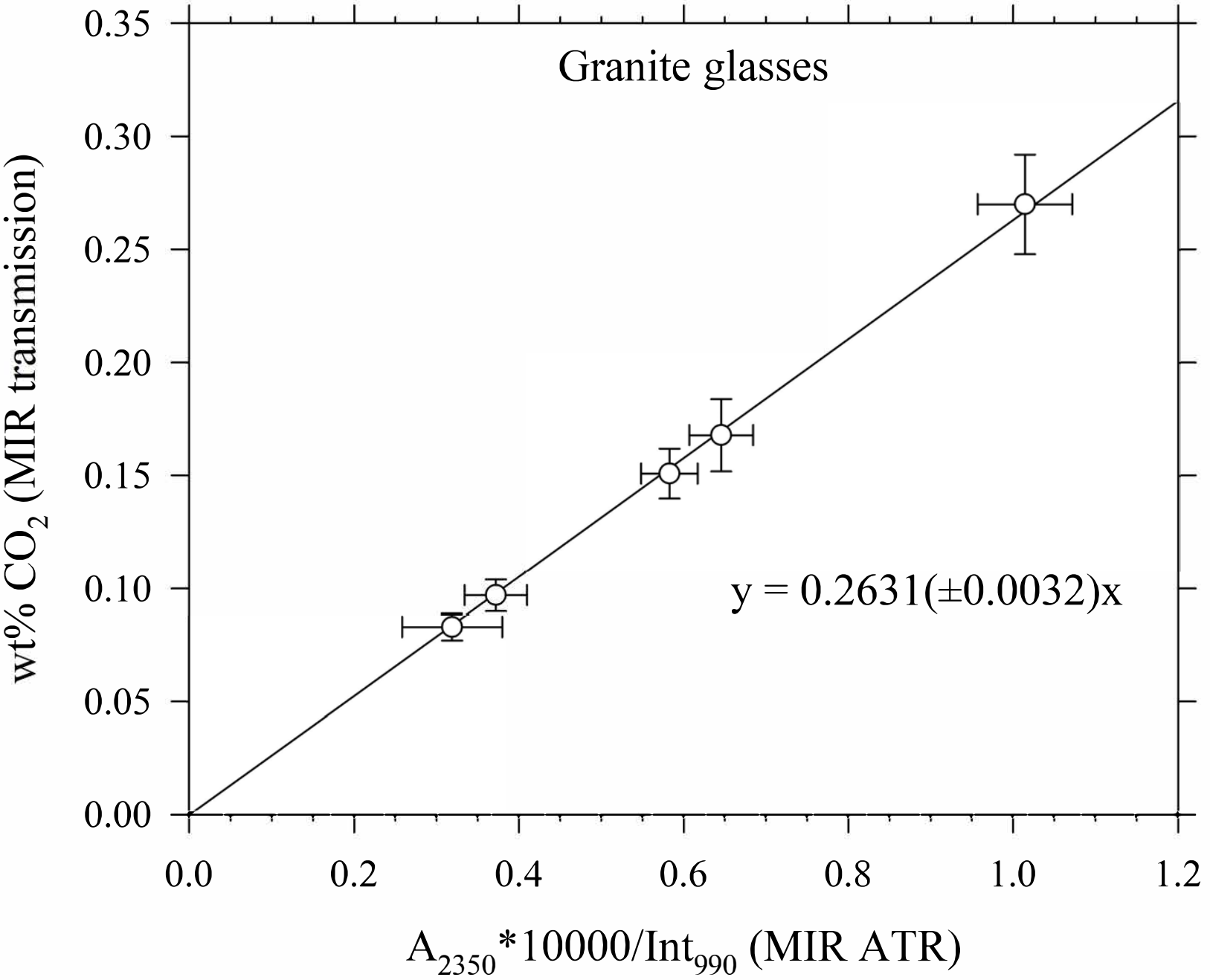
Granite glasses
y = 0.2631(±0.0032)x
wt% CO_2 (MIR transmission)
A_{2350}*10000/Int_{990} (MIR ATR)
0.00
0.05
0.10
0.15
0.20
0.25
0.30
0.35
0.0
0.2
0.4
0.6
0.8
1.0
1.2

Fig. 10

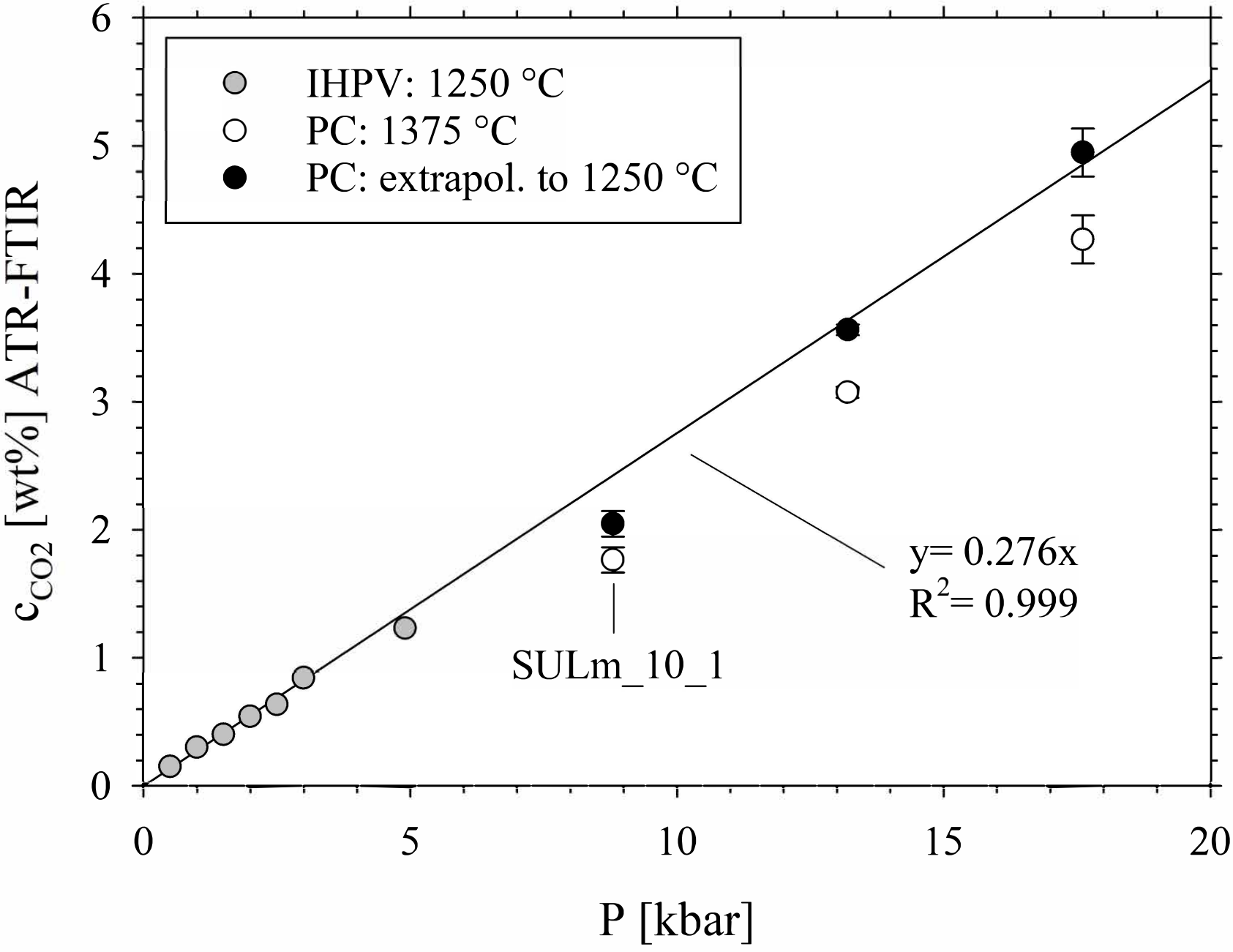
IHPV: 1250 °C
PC: 1375 °C
PC: extrapol. to 1250 °C
y= 0.276x
R2= 0.999
SULm_10_1
cCO2 [wt%] ATR-FTIR
P [kbar]
0
1
2
3
4
5
6
0
5
10
15
20

Fig. 11

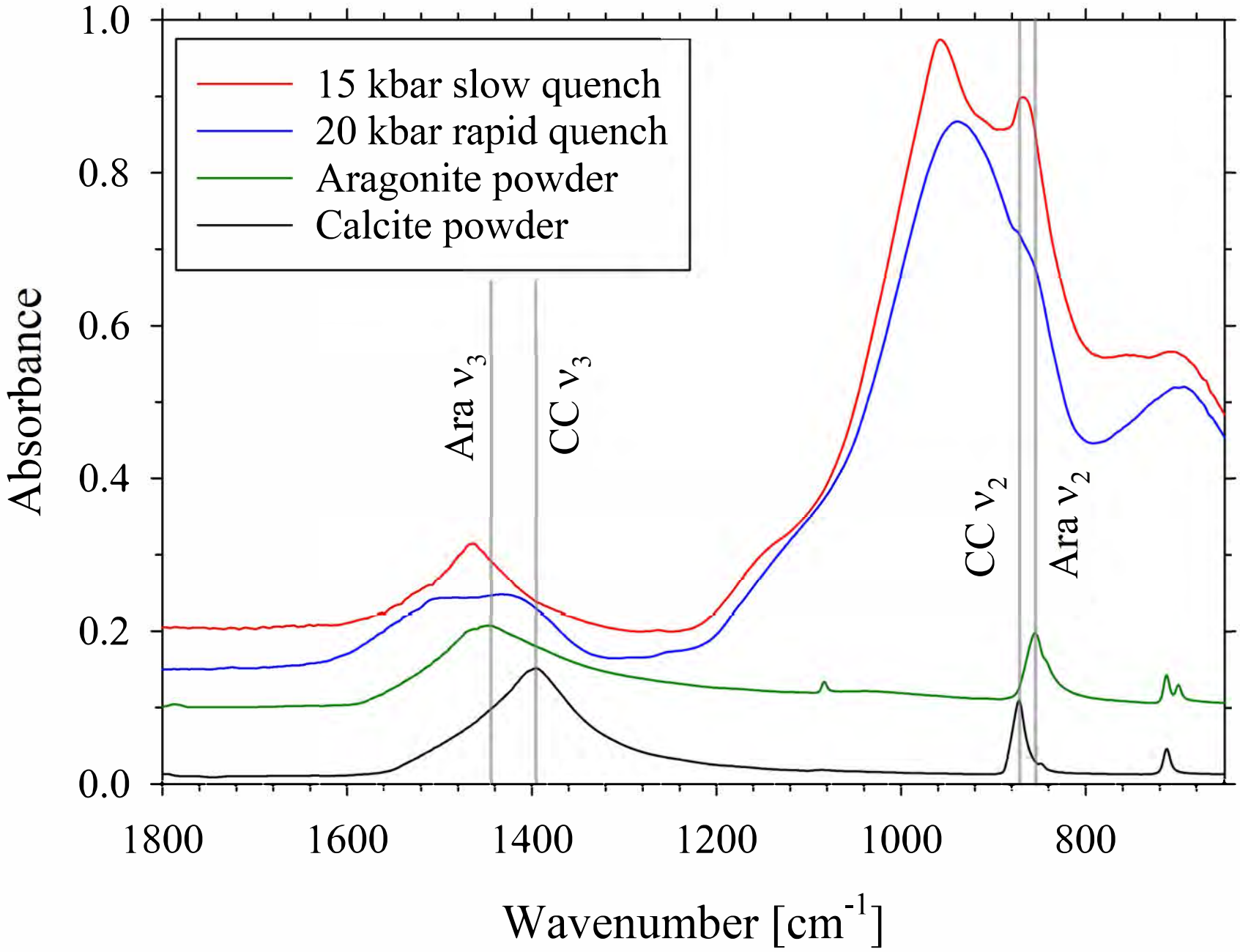
15 kbar slow quench
20 kbar rapid quench
Aragonite powder
Calcite powder
Ara ν3
CC ν3
CC ν2
Ara ν2
Absorbance
Wavenumber [cm-1]
1.0
0.8
0.6
0.4
0.2
0.0
1800
1600
1400
1200
1000
800